TÜBİTAK

Turkish Journal of Earth Sciences

http://journals.tubitak.gov.tr/earth/

Research Article

Turkish J Earth Sci
(2020) 29: 325-346

doi:10.3906/yer-1906-7

Geochemical and industrial properties of the Kejal kaolin deposit, NW Iran

Tohid NOURI[1,*], **Rahim MASOUMI**[2]

[1]Faculty of Engineering, University of Mohaghegh Ardabili, Ardabil, Iran
[2]Department of Earth Sciences, University of Tabriz, Tabriz, Iran

Received: 09.06.2019 • **Accepted/Published Online:** 24.10.2019 • **Final Version:** 15.01.2020

Abstract: The Kejal kaolin deposit, situated in the northwest of Iran, is considered a small part of the Hashtjin hydrothermal zone. The kaolinization process in this deposit has occurred in ignimbritic and volcanic tuff parent rocks in different grades such that severely kaolinized samples can be found in the middle section of the kaolinization profile. Kaolinite is the most abundant clay mineral in the studied samples. Quartz and cristobalite are the main minerals while anatase is the minor mineral of the kaolin samples. Among the major oxides, SiO_2, Al_2O_3, and TiO_2 show the highest concentrations in kaolin samples. The mass change calculations based on Ti show enrichment of Si, Al, Sr, and LREEs and depletion of alkali and alkali earth elements, HREEs, and HFSEs. The evaluation of REEs normalized to chondrite represents the higher concentration of LREEs comparing to HREEs. A remarkable positive Gd anomaly is seen in spider diagrams, which can be attributed to the primary CaO in the composition of ignimbritic precursor and also the Gd release due to the decomposition of Gd complexes and adsorption by clay minerals. The Eu negative anomaly is the other obvious characteristic of the studied samples and is most likely related to the alteration of feldspars, decomposition of plagioclase, and Eu liberation from the system. The significant positive correlations between REEs and Al_2O_3, TiO_2, and P_2O_5 demonstrate the important role of clay minerals, REE-bearing phosphate minerals such as monazite, and titanium minerals like anatase and rutile in the kaolinization process and REE transport and establishment. The performed particle size test based on the hydrometer method shows about 20% of particles <2 μm and 36%-42% of particles <25 μm, which reveals a dominant medium particle size for these kaolin samples. Furthermore, the chemical composition of the analyzed samples represents around 20% alumina. Based on the obtained physicochemical evaluations, the Kejal kaolin deposit is medium- to low-grade kaolin, which is useable after simple processing in the paper industry as filler and in the ceramic industry as floor tiles.

Key words: Argillic alteration, geochemistry, industrial properties, kaolin, Kejal

1. Introduction

Kaolin has been one of the important industrial minerals and is frequently utilized in many aspects of our lives (Bundy, 1993). Kaolin, which comprises predominantly kaolinite, has unique properties such as crystalline morphology, natural whiteness, fine particle size, nonabrasiveness, low surface area, cation exchange capacity, softness, and chemical stability (Kuşcu and Yıldız, 2016).

Kaolin deposits have been extracted and mined historically. Kaolin is used as a raw material in the ceramic, paper, paint, rubber, abrasive, and pharmaceutical industries (Murray, 1991; Manju, 2002). Kaolin quality changes from one deposit to another. In this regard, utilization potentials of a kaolin deposit depend on factors such as chemical composition (Al, Si, and iron oxide concentrations) and the color index. Kaolin deposits are found in primary (residual) and secondary (sedimentary) types (Prasad et al., 1991; Murray and Keller, 1993).

The kaolin resources of Iran have a wide distribution throughout the country. Hydrothermal kaolin deposits are found at many points, such as the northwest and southeast of the Iranian plateau, while sedimentary kaolin deposits are seen in central Iran and associated with huge sedimentary basins.

Hydrothermal alterations caused by Tertiary volcanic activities are observable in many parts of NW Iran (Figure 1). For example, the Tarom-Hashtjin alteration zone is considered as one of the most significant mineralized zones in Iran. This altered zone, which has experienced Tertiary magmatism and volcanism, has a high distribution of metallic mineralizations such as Cu, Pb, Zn, Fe, Au, and Ag and nonmetallic deposits such as kaolin, bentonite, zeolite, and perlite.

There are some kaolinized spots in the Tarom-Hashtjin altered zone, with the Kejal kaolin deposit being the most important one having medium- to high-quality kaolin

* Correspondence: t.nouri@uma.ac.ir

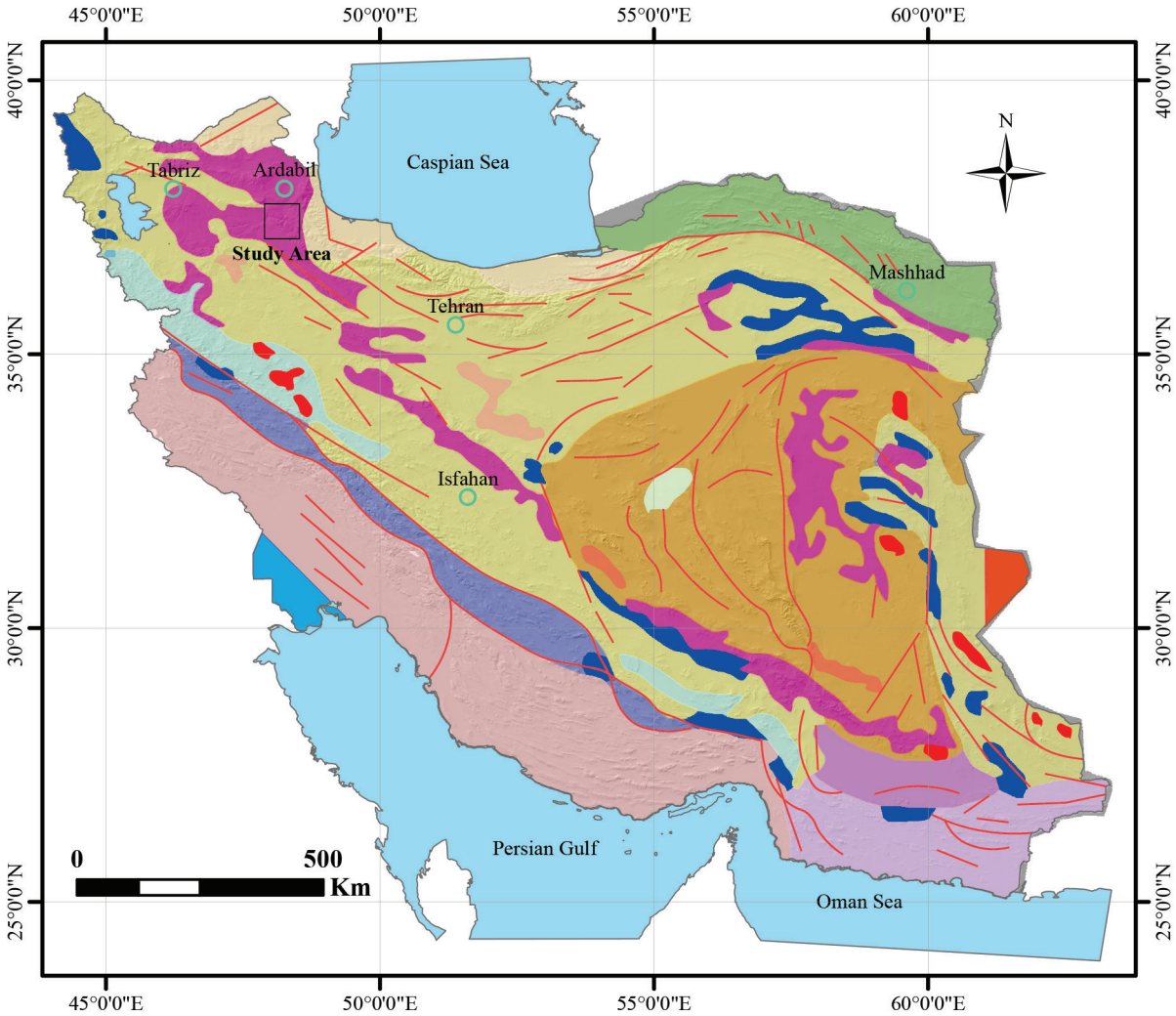

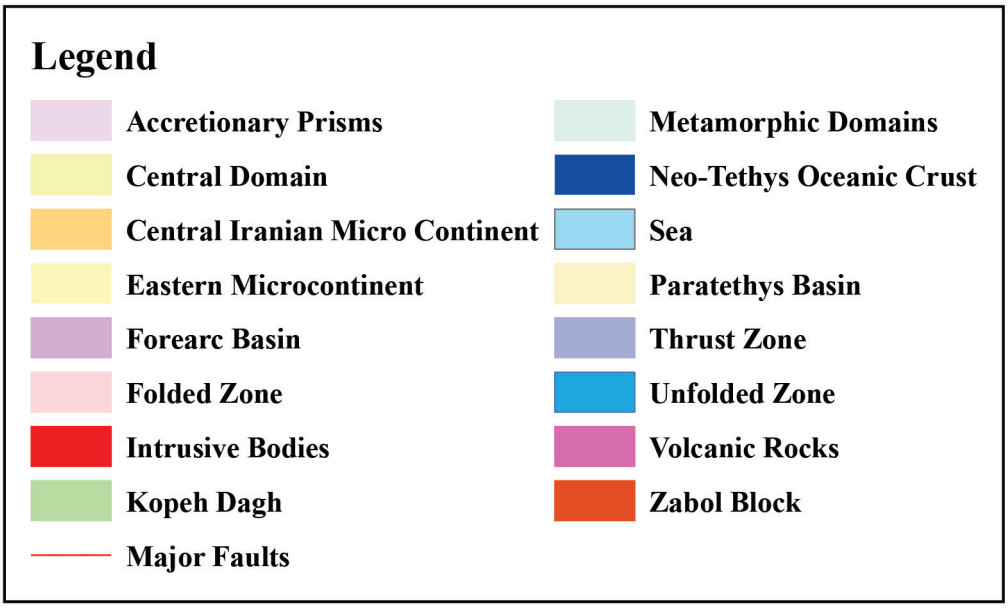

Figure 1. Geological map of Iran representing the main structural zones of Iranian plateau (modified after Aghanabati, 2004), with location of study area and adjacent cities.

outcrops. Despite this study and those conducted by Masoumi (2010) and Abedini et al. (2011), little is known about the Kejal kaolin.

Most of the previous studies in this area were either general geological studies or are not related to the kaolins of the area. Faridi and Anvari (2000) studied the geology of the Hashtjin area in detail and prepared the geological map of this area in 1:100,000 scale. Hajalilou (1999) and Moayed (2001) studied the geology of the area from petrological and mineralization points of view. Moghadami (2011) investigated the zeolite occurrences in the Kejal area.

With regard to high demands for kaolin as a raw material in many industries such as paper and ceramic manufacturing, the identification of high-quality kaolin deposits is a requirement in order to supply the required kaolin for these industries and also to classify the existing kaolin resources based on their quality and appropriate uses.

Considering the importance of the Kejal kaolin deposit, the authors of the present work attempted to evaluate the Kejal deposit from the geochemical and application points of view. These evaluations will lead us to identify the quality of this kaolin deposit and determine the most suitable application fields for this deposit.

2. Geological setting

The Tarom-Hashtjin area is located in the western part of the Alborz range. According to the latest structural classifications of the Iranian plateau, this area is considered as a subzone under the Alborz-Azerbaijan structural zone (Stocklin, 1977; Alavi, 1996). The Tarom-Hashtjin subzone is characterized by its gentle thrusts with a SW trend and a considerable increase in crust thickness in the NE-SW direction. These geological events are the result of a quick uplift due to Austrian orogeny, which might be evidenced by movements of the Gizilozan valley. The Kejal-Shamsabad alteration zone covers an area of ~25 km^2 around the Gizilozan valley and includes different types of chloritic-sericitic-argillic-silicic alterations (Hajalilou, 1999). The parent rocks of these alterations in many points are volcanic tuff, ignimbrite, andesite-basalt, volcanic breccia, and rhyolites. The excessive hydrothermal silica precipitations are the main characteristics of this zone.

These units are usually observable in white, yellow, and lime colors. The yellow and lime colors are the result of pyrite decomposition and the presence of abundant sulfur in altered zones. The sulfur content of some units reaches 32,000 ppm. Geologically, the study area shows the characteristics of a volcanic setting including volcanic tuffs, ignimbrite, and trachyandesite lavas. Alteration as a remarkable feature in lithological units has covered a vast area and developed in tuffaceous and ignimbritic units more than trachyandesites (Figure 2a). The age of these units is Eocene (Faridi and Anvari, 2000).

Field observations show several faults with different trends in the study area. The injection of hydrothermal fluid along these faults and fractures has caused the formation of kaolin from the ignimbritic parent rock (Figures 2a, 2b, and 3a–3d). Alteration-related textures such as Liesegang rings or Cockade structures are easily visible in different parts of the area (Figure 3e). These textures are often created by rhythmic precipitations controlled by fissures and cracks, which act as conduits for the hydrothermal solutions. The rings are different in chemical composition and the red-colored rings are usually Fe-rich layers (Masoumi, 2010). In some parts of the kaolinized zone, massive outcrops of silica sinter are seen. This sinter contains fine-grained minerals such as opal and cristobalite. However, large crystals of quartz (1.5 cm) in a medium-sized quartz context (2 mm) can also be identified in the Kejal mining area, which are suitable for fluid inclusion studies.

3. Materials and methods

After detailed fieldwork and frequent observations of lithological properties, fault and fracturing systems, and existing alterations, the geological map of the area was prepared in the local scale and sampling was done via both systematic and random methods. The most suitable samples were selected for chemical analysis and petrographic studies. Sampling was carried out along a profile of ~200 m across the kaolin deposit. A total of 10 samples were taken from the kaolinized zone at 10-m intervals on the basis of changes in their physical characteristics. The selected samples were dried, ground in an agate mortar, sieved, and prepared for analysis.

The mineralogy of the parent rock was determined by examining thin sections under a polarizing microscope. For the identification of mineral phases for clayey and nonclayey minerals, identification analyses were done using X-ray powder diffraction (XRD) analyses (diffractometer model: Philips-Xpert Pro) at the Iran Mineral Processing Research Center.

The major and minor oxides and trace elements were determined via inductively coupled plasma emission spectrometry (ICP-ES). Rare earth element (REE) contents were determined by inductively coupled plasma mass spectrometry (ICP-MS) at the ALS Chemex Laboratory (Vancouver, Canada) with 0.1–0.2 ppb detection limits. Some other samples were analyzed using X-ray fluorescence (XRF; Philips PW1480) in the laboratory of the Iranian Geological Survey.

The LOI values were measured in the mentioned laboratory by ignition of the samples (1000 °C for 1 h). The SEM images were taken using a VEGA TESCAN-LMU and FESEM MIRA3 TESCAN-XMU in the Razi Metallurgical Research Center of Iran. These images were taken at an

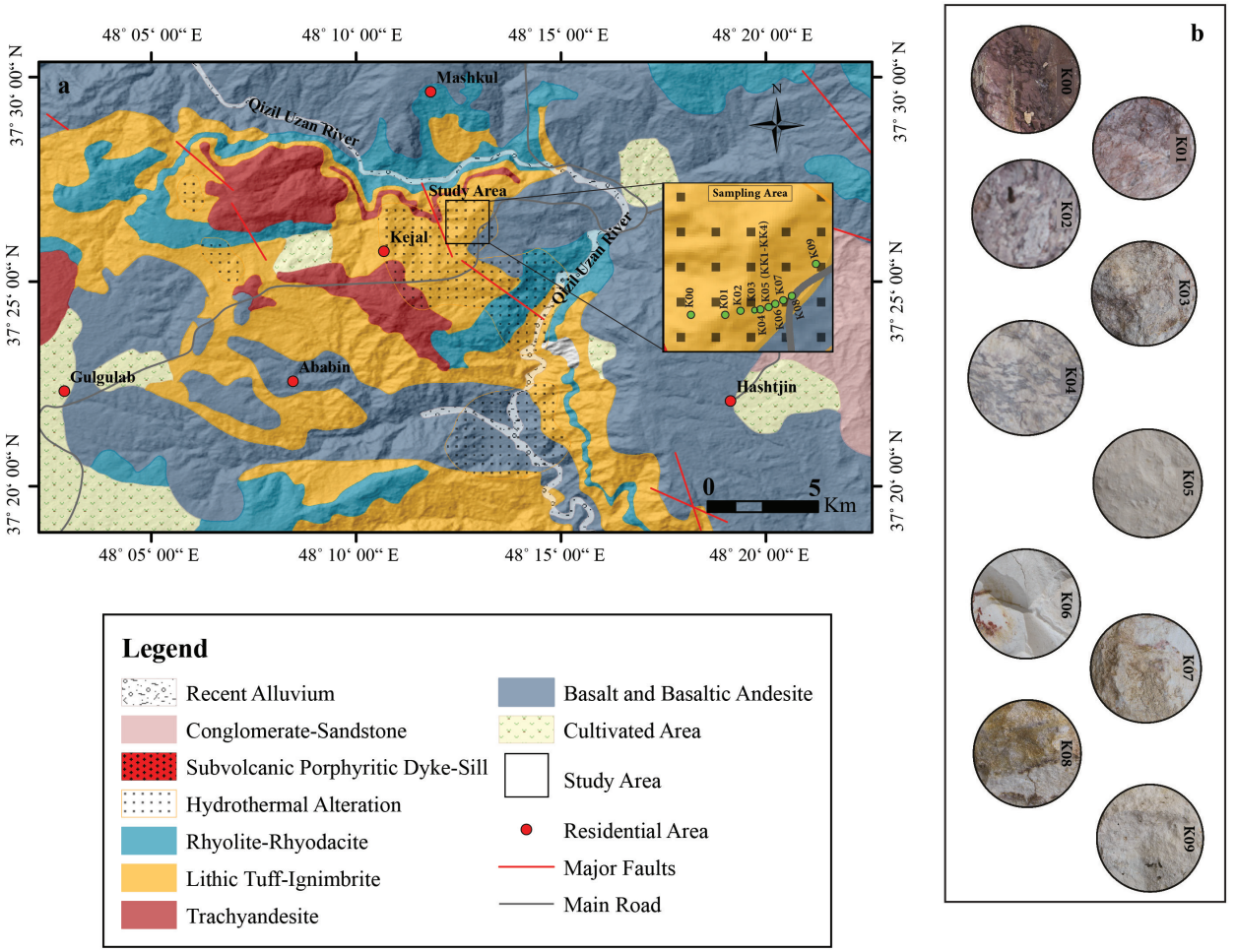

Figure 2. a) Geological map of the study area representing the lithological units, alteration zones, and major faults; b) hand specimen photos of the analyzed samples showing the color variation of kaolin in the study area.

accelerating voltage of 3–30 kV controlled by the VEGA TC.

In order to obtain the particle sizes of the studied samples, the prevalent hydrometer method was used in this study. Two samples from the pure kaolin unit (KK1 and KK4, close to the K05 sampling point) were selected for particle size testing. To measure the weight of the samples a scale with sensitivity of 0.01 g was used. A No. 10 sieve (2 mm) was used in the primary preparation of the powders. A sedimentation cylinder with height of 457 mm and diameter of 63.5 mm was also used in this process. The sensitivity of the used thermometer was half of a degree in Celsius and sodium hexametaphosphate was used as a dispersing agent (ASTM, 1998).

4. Results

4.1. Petrography and mineralogy

Ignimbrite, as the precursor rock of the kaolinized unit, has a considerable outcrop in the west of the kaolinized zone (Figures 2a and 2b). Kejal ignimbrite is red-brown in color (Figures 3a and 3d) and shows a welded texture in hand specimens and eutaxitic texture in the rock context. Although this ignimbrite unit has experienced severe kaolinization, fairly fresh and least altered samples were prepared for petrography and microscopic studies. The ignimbrite samples show large euhedral K-feldspar crystals in a glassy context under the microscope. Plagioclase is present in phenocryst and needle shapes and is often accompanied by clinopyroxene (augite) (Figures 3f, 3g, and 3h). Volcanic glass is one of the main constituents of the parent rock and in some cases makes up 40% to 50% of the whole thin sections (Figures 3f, 3g, and 3h). Pyrite is the only metallic mineral observed in the altered samples (Figures 3h and 3i).

Trachyandesite lava flow is another main lithological unit in the study area. This rock type is texturally porphyritic and vitrophyric. Phenocryst and needle-shaped plagioclases are obviously seen in the thin

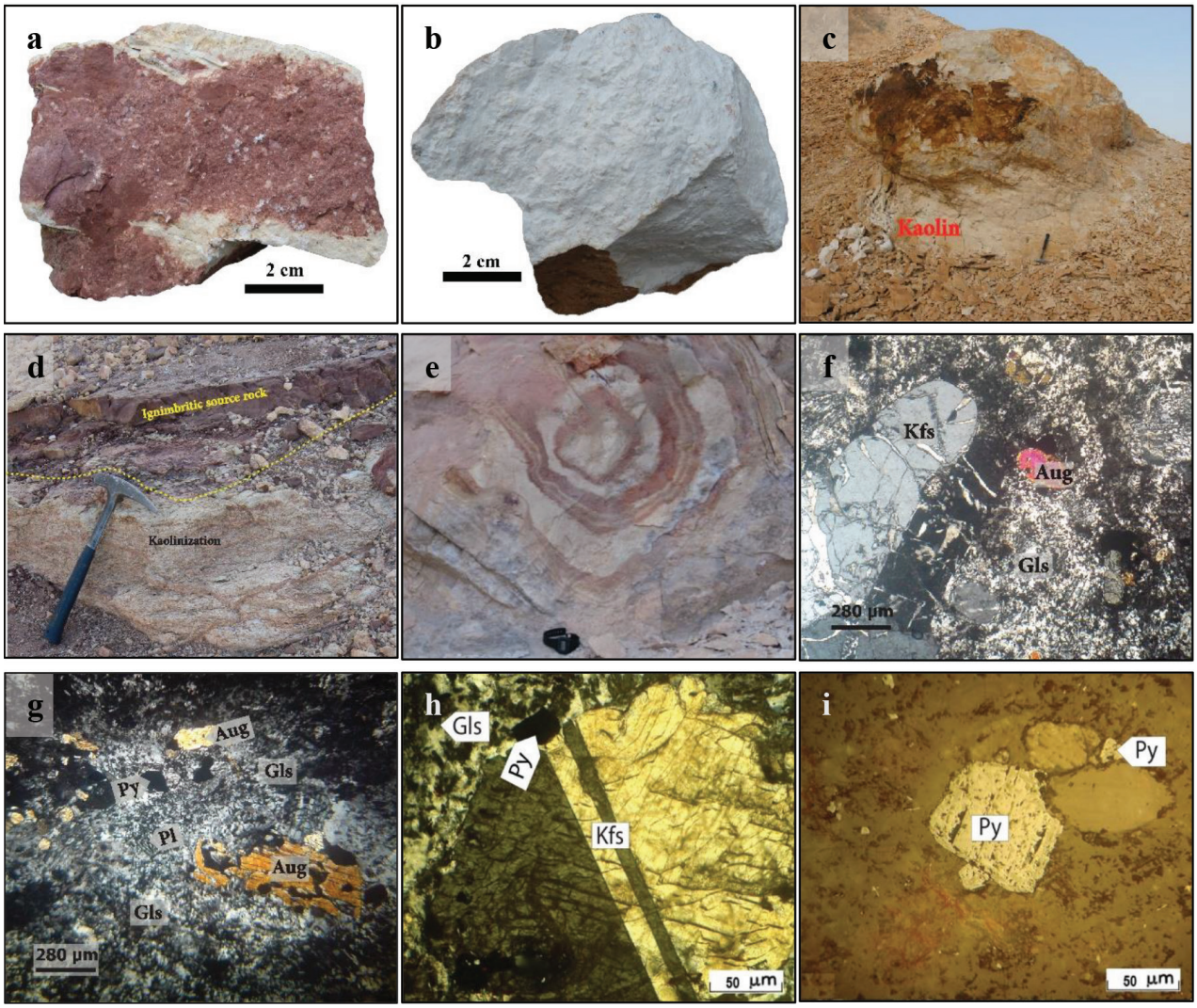

Figure 3. Photos related to the Kejal kaolin deposit. a) Semikaolinized sample from Kejal area; b) pure kaolin sample from Kejal deposit; c) massive kaolin body in Kejal kaolin mine; d) process of kaolinization in Kejal ignimbrite; e) Leisegang structure in the alteration zone representing rhythmic precipitations controlled by fissures and cracks; f) ignimbrite microphotograph showing plagioclase phenocryst in a volcanic glass context (XPL); g) ignimbrite microphotograph representing the decomposition of augite crystal in a glassy context (XPL); h) ignimbrite microphotograph showing K-feldspar, glass, and pyrite (XPL); i) ignimbrite microphotograph representing pyrite (PPL).

sections (Figure 3g). The plagioclases are compositionally oligoclase-andesine. Augite is also present in thin sections as a minor constituent (Masoumi, 2010).

The kaolin unit, which is considered as the main ore body in the study area, represents a white to brown color spectrum. The colors change from the hydrothermal fluid conduits outward such that the purest samples of kaolin are white in color (Figure 3b) and semialtered samples appear red or brown (Figures 3a and 3d).

Based on the XRD analyses, the main mineral assemblages of the studied samples consist of kaolinite, quartz, cristobalite, and anatase (Figures 4a and 4b). In the K02, K03, and K05 samples, which were taken from fully altered ignimbrite (pure kaolin), kaolinite is the main clay mineral. Quartz and cristobalite are found associated with kaolinite. As mentioned, plagioclase and K-feldspar are abundant in the ignimbritic precursor rock. Regarding the low resistance rates of these minerals against hydrothermal alteration, these minerals are easily altered to clay minerals, especially to kaolinite. The high frequency of silica polymorphs (quartz and cristobalite) is also obvious. This frequency can be related to the silicification of the altered units, which has caused the formation of mass silica bodies and even quartz crystals (1.5 cm) throughout the argillic alteration zone. Anatase is also seen as a minor mineral on XRD graphs. Figures

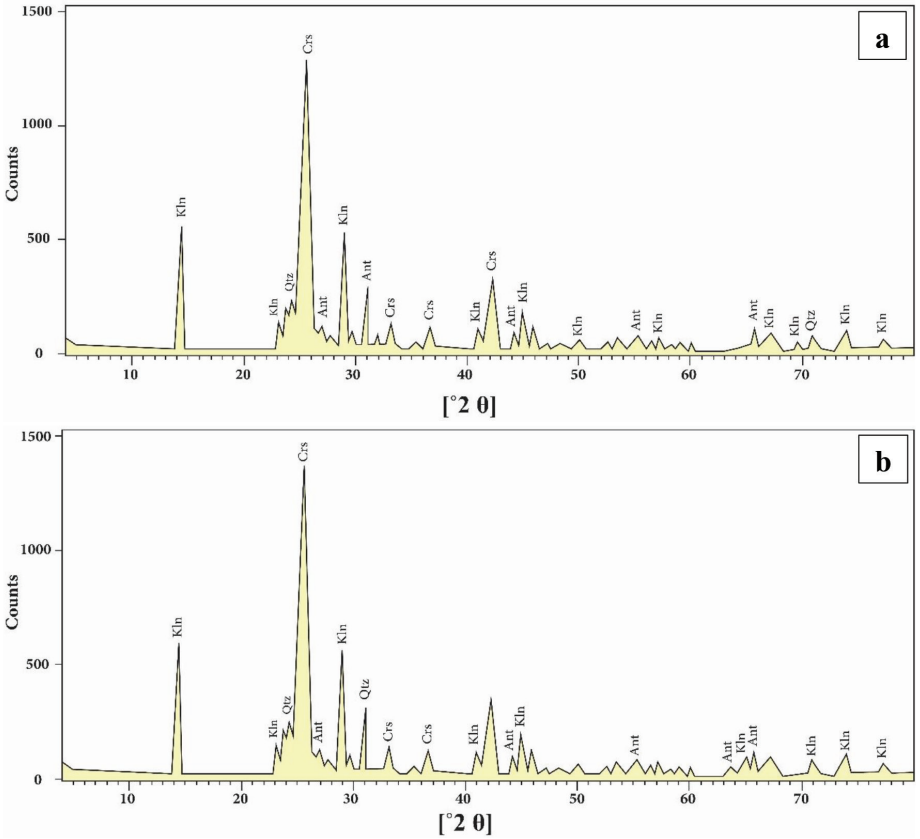

Figure 4. a, b) XRD patterns of selected samples from fully altered ignimbrites (kaolin) from the study area. Kln (kaolinite); Qtz (quartz); Crs (cristobalite); Ant (anatase).

4a and 4b represent the XRD graphs of the studied kaolin samples.

Among the fully altered kaolin samples, the purest samples were selected for SEM studies. There is apparent concordance between the recognized minerals in electron microscope images and XRD results. The prepared SEM microphotographs are shown in Figures 5a–5d (KK1) and Figures 6a–6d (KK2). Kaolinite pseudohexagonal crystals and booklets of kaolinite are seen in Figures 5a and 5b. Fracture filling with kaolinites is observable in some cases (Figure 5b). Flaky kaolinite is also present (Figures 5c and 5d). White spheroidal particles are also observed on kaolinite crystals (Figures 5c and 5d). These particles are most likely cristobalite, which has also been detected in XRD analyses. The pyramidal and prismatic crystals are seen in Figures 6a–6c. These crystals are likely quartz, which is formed along veins and fractures.

4.2. Chemical analysis

The results of the chemical analysis are shown in Table 1. These analyses reveal major oxides, trace elements, and REEs of the kaolinized unit and ignimbritic precursor. The analysis of ignimbrite yields SiO_2 = 54.5, Al_2O_3 = 15.4, Fe_2O_3 = 6.05, CaO = 4.75, K_2O = 2.95, Na_2O = 2.79, MgO = 2.44, and TiO_2 = 0.76 wt.%. The main share of these elements has been removed during hydrothermal leaching. Although during the alteration process the concentration values of elements have been changed, concentration patterns with little changes are the same.

4.3. Physical properties

The physical properties of kaolins along with chemical characteristics of this ore mineral are important and the assessment of these parameters is necessary in order to determine their industrial applications. In this study, some physical parameters such as particle size, specific gravity, moisture content, natural and dry weight, saturated weight, volume of sample, water absorption, and viscosity were calculated and measured.

4.4. Particle size

The particle size distribution of clay minerals in kaolin samples is one of the main parameters to distinguish the applications of this material. The particle size of clays plays an important role in ceramic resistance, the shrinkage of kaolin paste, and its use for filler, coatings,

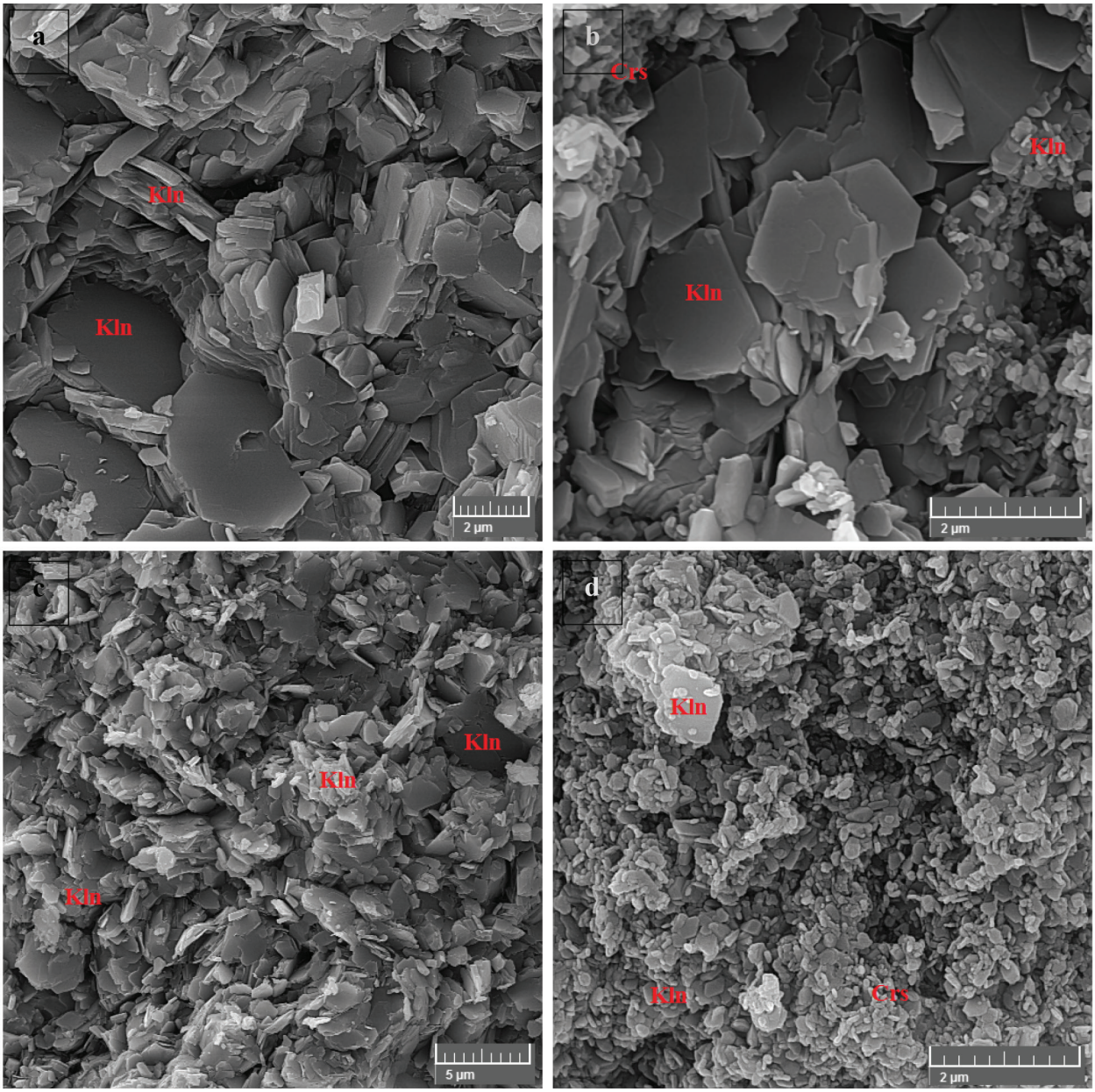

Figure 5. Scanning electron microscopy (SEM) photomicrographs representing the existing minerals in the studied kaolin samples (KK1). a) Pseudohexagonal crystals of kaolinite (Kln) and kaolinite booklets; b) pore-filling crystals of platy kaolinite; c, d) flaky crystals of kaolinite (Kln).

and glossiness in the paper industry (Aref and Lei, 2009).

Ryan (1978) and Vegliò et al. (1996) stated that the finer particles of kaolinite have great importance in the paper industry, as filler and coatings, in pharmaceuticals, and in the ceramic industry. The kaolin used in such cases should have particle size of 1–50 µm (Heinskanen, 1996).

The calculated particle size for the studied samples using the hydrometer method is presented in Figures 7a and 7b. To obtain the particle size of the samples, a simplified equation for Stokes' law has been used (ASTM, 1998).

$$D = K\sqrt{(L/T)}$$

Here, D is particle diameter in mm; L is the distance of the level at which the density of the suspension is measured from the surface of the suspension (in cm), also known as effective depth; T is time elapsed from the beginning of the test until the time the reading is made in min; and K is a constant depending on the specific gravity of the soil

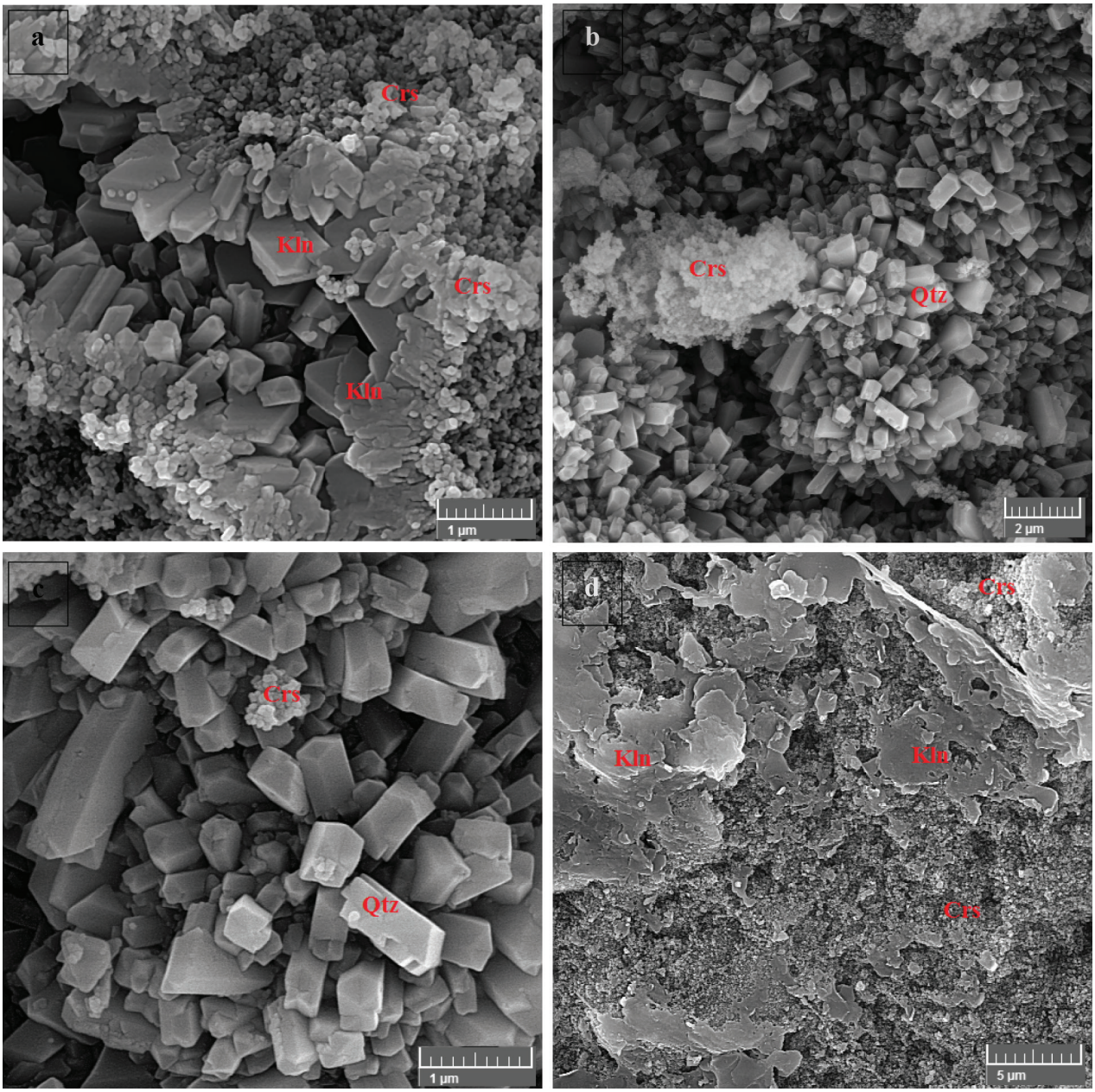

Figure 6. Scanning electron microscopy (SEM) photomicrographs representing the existing minerals in the studied kaolin samples (KK4). a) Quartz (Qtz) associated with spheroidal silica minerals (cristobalite (Crs) or Opal?) and kaolinite (Kln); b, c) pyramidal quartz (Qtz) and spheroidal silica minerals (cristobalite (Crs) or opal?); d) flaky kaolinite (Kln) plates.

particles and the temperature of the suspension (ASTM, 1998).

The obtained results from hydrometer analyses are provided in Table 2 and Figures 7a and 7b. As seen there, the acquired particle sizes for the studied samples represent medium-sized particles. The particle size distribution range for KK1 is 0.8–25 µm and for KK4 it is 0.76–33 µm. The frequency of particles of <2 µm among the studied samples is slightly more than 18%.

4.5. Other parameters

Other parameters such as specific gravity, moisture content, natural and dry weight, saturated weight, volume of the sample, water absorption, and viscosity were also calculated and measured for the studied samples. These parameters are listed in Table 3. The measured specific gravity for the KK1 and KK4 samples are 2.45 and 2.62, respectively, as measured at 20 °C. The moisture contents of these samples are 0.379% and 0.866%. The obtained natural

Table 1. ICP-MS analysis results of Kejal kaolin samples showing major oxides, REEs, and trace elements; hyphen represents not measured elements.

Samples		SiO_2 (wt.%)	Al_2O_3 (wt.%)	Fe_2O_3 (wt.%)	CaO (wt.%)	Na_2O (wt.%)	K_2O (wt.%)	TiO_2 (wt %)	MgO (wt.%)	MnO (wt.%)	P_2O_5 (wt.%)	Cr_2O_3 (wt.%)	SrO (wt.%)
Ignimbrite	K00	54.5	15.4	6.05	4.75	2.79	2.95	0.76	2.44	0.12	0.21	0.01	0.04
Semialtered	K01	69.4	15.75	4.78	0.17	0.04	0.11	0.63	0.12	<0.01	0.07	0.01	0.09
Semialtered	K02	68.9	16.45	3.44	0.22	0.13	0.53	0.6	0.46	0.02	0.2	0.01	0.09
Semialtered	K03	69.3	18.15	1.18	0.19	0.02	0.04	0.55	0.04	<0.01	0.21	0.01	0.21
Semialtered	K04	67.2	19.2	2.72	0.22	0.02	0.03	0.73	0.02	<0.01	0.2	<0.01	0.12
Fully altered	K05	82	10.6	0.32	0.12	0.02	0.05	0.86	0.01	<0.01	0.03	<0.01	0.01
Fully altered	K06	95.8	1.6	0.06	0.11	0.07	0.07	1	0.01	<0.01	0.02	<0.01	<0.01
Semialtered	K07	71.6	17.7	0.17	0.18	0.01	0.03	1.08	0.02	<0.01	0.03	<0.01	<0.01
Semialtered	K08	80.8	4.66	8.05	0.17	0.05	0.08	0.9	0.04	<0.01	0.09	0.01	0.06
Fully altered	K09	79.4	10.8	0.3	0.17	0.06	0.24	0.81	0.02	<0.01	0.51	0.02	0.39
Fully altered	K10	71.62	17.55	1.97	0.13	0.05	0.04	0.001	0.01	0.014	0.241	0.0075	0.6423
Fully altered	K11	74.62	15.51	2.31	0.15	0.01	0.01	0.005	0.01	0.012	0.129	0.0118	0.4769
Samples		La (ppm)	Ce (ppm)	Pr (ppm)	Nd (ppm)	Sm (ppm)	Eu (ppm)	Gd (ppm)	Tb (ppm)	Dy (ppm)	Ho (ppm)	Er (ppm)	Tm (ppm)
Ignimbrite	K00	24.1	48.6	5.4	20.1	4.04	1.1	14.7	0.69	3.93	0.82	2.55	0.35
Semialtered	K01	27	50	5.3	18	2.7	0.53	17.2	0.39	2.68	0.57	1.94	0.32
Semialtered	K02	39.3	74.8	8.04	28.7	5.43	1.35	17.7	1.18	8.46	1.92	6.41	0.95
Semialtered	K03	29.8	56.1	7.23	33.3	7.11	1.32	27.6	0.73	3.49	0.67	2.24	0.33
Semialtered	K04	37.4	72.2	8.32	32.3	6.22	1.73	19.3	0.88	4.03	0.64	1.94	0.26
Fully altered	K05	20.8	35.3	3.26	9.9	1.9	0.23	11.8	0.33	1.87	0.36	1.21	0.19
Fully altered	K06	2.9	5.8	0.61	2.1	0.38	0.05	2	0.08	0.51	0.11	0.39	0.07
Semialtered	K07	11.8	20.1	1.99	6.5	1.77	0.29	18.5	0.48	3.31	0.74	2.51	0.43
Semialtered	K08	27.2	33.2	3.19	10.4	2.04	0.43	27	0.23	1.59	0.38	1.5	0.26
Fully altered	K09	89.1	138	12.05	35.5	5.36	1	30.7	0.46	1.76	0.29	0.94	0.14
Fully altered	K10	21	95	-	-	-	-	-	-	-	-	-	-
Fully altered	K11	16	100	-	-	-	-	-	-	-	-	-	-
Samples		Lu (ppm)	V (ppm)	Cr (ppm)	Co (ppm)	Ni (ppm)	Cu (ppm)	Zn (ppm)	Mo (ppm)	Ag (ppm)	Ta (ppm)	W (ppm)	Rb (ppm)
Ignimbrite	K00	0.39	153	70	17.6	20	33	46	<2	<1	1	5	93.6
Semialtered	K01	0.34	130	60	1.3	8	8	<5	5	<1	1.7	6	7.3
Semialtered	K02	1.02	84	40	2.6	7	12	26	4	<1	1.8	4	19.2
Semialtered	K03	0.34	295	60	<0.5	<5	<5	<5	<2	<1	1.7	3	3.9
Semialtered	K04	0.27	96	40	0.9	<5	<5	6	3	<1	2	4	3
Fully altered	K05	0.21	29	10	<0.5	<5	7	5	2	<1	2.7	4	7.7
Fully altered	K06	0.08	17	10	<0.5	<5	<5	5	<2	<1	2.2	2	12
Semialtered	K07	0.5	33	10	<0.5	<5	<5	11	2	<1	3.7	3	4
Semialtered	K08	0.28	162	90	5.5	6	77	22	16	<1	1.7	2	6.2
Fully altered	K09	0.16	90	130	<0.5	<5	10	9	2	<1	1.3	2	8.5
Fully altered	K10	-	127	-	4	1	6	31	< 5	-	-	<5	2
Fully altered	K11	-	156	-	8	6	4	42	285	-	-	<5	7

Table 1. (Continued).

Samples		Cs (ppm)	Ba (ppm)	Y (ppm)	Zr (ppm)	Nb (ppm)	Hf (ppm)	Pb (ppm)	Sn (ppm)	Th (ppm)	Tl (ppm)	U (ppm)	Ga (ppm)
Ignimbrite	K00	1.5	429	22.7	206	13.8	5.1	<5	1	8.35	<0.5	2.09	14.7
Semialtered	K01	1.21	99.8	14.8	300	22.5	7.4	<5	3	13.6	<0.5	3.08	17.2
Semialtered	K02	1.81	217	56.8	319	24	8.3	25	3	16.6	<0.5	3.41	17.7
Semialtered	K03	1.87	178	17.5	288	22.4	7.6	39	2	12.7	0.5	2.58	27.6
Semialtered	K04	1.54	134	16.4	372	27.6	9.6	26	7	18.5	<0.5	3.54	19.3
Fully altered	K05	4.66	43.5	10.9	449	37.3	11.6	<5	4	14.75	<0.5	5.02	11.8
Fully altered	K06	6.42	38.8	3.6	216	37	6.1	<5	2	4.05	<0.5	1.58	2
Semialtered	K07	4.25	27.9	20.4	675	60.5	17.3	7	7	26.1	<0.5	4.67	18.5
Semialtered	K08	3.03	154.5	11.7	291	21.7	7.3	36	17	21.5	<0.5	6.98	27
Fully altered	K09	3.76	468	6.2	224	19	5.9	42	1	26.6	<0.5	3.6	30.7
Fully altered	K10	-	-	24	1318	-	-	42	-	14	-	2	60
Fully altered	K11	-	-	21	1202	-	-	43	-	10	-	2	53

Table 2. The particle size distribution values of studied kaolin samples.

KK1		KK4	
Particle size (μm)	Frequency (%)	Particle size (μm)	Frequency (%)
0.8	16.8	0.76	17.1
1.4	17.85	1.3	18.1
3.3	22.05	3.1	20.12
6.6	26.25	6.3	22.12
9.1	29.4	8.9	24.14
12.4	32.55	12.6	26.12
19.0	38.85	21.2	32.18
25.0	42	33	36.2

and dry weights and the saturated weight of the KK1 and KK4 samples are 42.16 g and 80.81 g, 42 g and 89.8 g, and 58.6 g and 89.8 g, respectively. The values measured for the volume of these samples are 39.5% and 12%. The water absorption amounts are 39.52% and 12.09% and the obtained viscosities of these samples are 37.9% and 39.3%.

Viscosity is one of the main characteristics of kaolin in the process of quality evaluation. The resistance offered by a fluid to flow when subjected to a speed gradient or shear stress is a function of its viscosity (De Noni et al., 2002). This is one of the major rheological properties of kaolin that determines its suitability in the paper, pulp, and paint industries. The paper production process requires adhesive slurries (dependent on viscosity) that can flow and give smooth, even coverage to coat papers and improve their surface properties. In this study, kaolin samples were made into slurries (50% solid) and their viscosities were determined using the workflow described by Beazley (1972).

The approach involves making kaolin slurries of different concentrations by progressive dilution with water and then measuring the viscosities with a viscometer. The measurements were made with a viscometer at a specific temperature of 20 °C. A specific temperature datum was chosen because the aggregation of clay particles is known to vary with temperature changes. The result of the analyses shows that the viscosity of Kejal kaolin samples ranges from 37.9 to 39.3 P as shown in Table 3. The viscosity of raw kaolin can be changed during processing. Low-viscosity kaolin slurries are needed in paper coating. As seen in Table 3, the prepared slurries from Kejal kaolin samples show low viscosity ranges (37.9–39.3 P). This range of

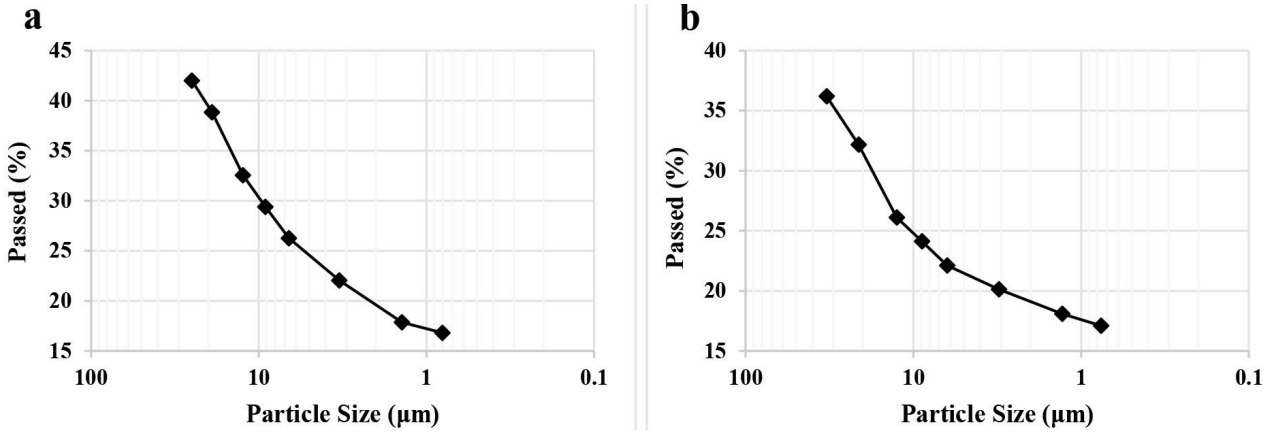

Figure 7. Diagrams showing the results of hydrometer tests. a) Sample KK1; b) sample KK4.

Table 3. The measured physical parameters for studied kaolin samples.

Sample no.	Specific gravity (20 °C)	Moisture content (%)	Natural weight (g)	Dry weight (g)	Saturated weight (%)	Volume of sample (mL)	Water absorption (%)	Viscosity of pulp (50% solid) at 20 RPM(Brookfield viscometer) (CP)
KK1	G20 = 2.45	0.379	42.16	42	39.5	30.2	39.52	37.9
KK4	G20 = 2.62	0.866	80.81	80.11	12	40.1	12.09	39.3

viscosity is suitable in the coating process, but if different degrees of viscosity are needed, the viscosity of the slurry will be changed using the change of particle size, pH, and solids and by adding special polymers (Qiu et al., 2017).

5. Discussion

5.1. Geochemistry

Among the major oxides, SiO_2, Al_2O_3, and TiO_2 show the highest concentration values in the kaolin samples (Figure 8). The concentration patterns in the kaolin samples have the following order: $SiO_2 > Al_2O_3 > Fe_2O_3 > TiO_2 > CaO > K_2O > Na_2O > MgO > P_2O_5$. During the hydrothermal alteration process, the alkali and alkali earth elements were removed from the parent rock (Figure 9a). The average SiO_2 value in analyzed samples is 73%. The highest concentrations of Al_2O_3 and TiO_2 are 19.2% and 1.08%, respectively. In general, the Al_2O_3 values in the purest and white kaolin samples should be in the highest amounts, but this rule does not apply in the studied samples.

All of the kaolin samples show a high SiO_2 content and suggest a silicification process that has affected the high-quality kaolins. This event could be due to the replacement of the parent material by Si instead of Al (Jiménez-Millán et al., 2008) during hydrothermal alteration. Figure 8 shows major oxide contents in the studied samples. As can be seen, SiO_2 and Al_2O_3 constitute the most important proportions of the composition of the whole samples. Figure 8 also represents the composition of Kejal kaolin compared to some kaolin samples around the world.

The major oxide variation patterns normalized to the composition of ignimbritic parent rock is shown in Figure 9a. The strong positive TiO_2 anomaly is clearly observable in this diagram. With a quick glance at TiO_2 values (Table 1), one can understand that no TiO_2 has been added to the primary values during kaolinization and the TiO_2 positive anomaly had been created due to its immobility. It is worth mentioning that the hydrothermal leaching process removes mobile elements such as Na, K, Ca, and

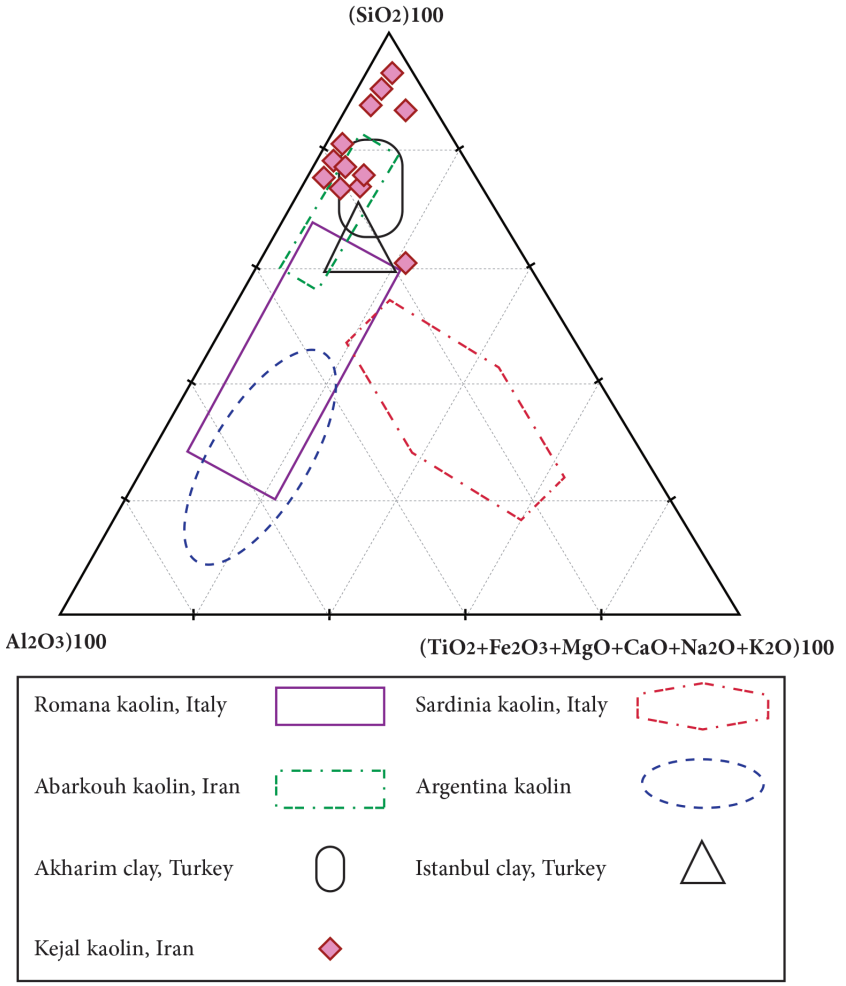

Figure 8. *(Al_2O_3), (SiO_2), and (TiO_2+Fe_2O_3+MgO+CaO+Na_2O+K_2O) ternary diagram showing the main oxide content in the studied samples and some other kaolin deposits around the world. Romana kaolins from Ligas et al. (1997); Sardinia clays from Strazzera et al. (1997); Abarkouh* kaolin *from Mahjoor et al. (2009); Argentine kaolins from Cravero et al. (1997); Akharım clays from Kuşcu and Yıldız (2016);* İstanbul *clays from Celik (2010).*

Mg and so the kaolin samples show the lowest values of such elements. These elements, which usually make up the structure of feldspar and mica (Galán et al., 2016), are released from the structure of the minerals under weathering conditions. This event can be the result of the negative anomaly of mobile elements in fully altered samples. The mean value of Fe_2O_3 is a key factor in the kaolin utilization industry. Kaolin samples with high Fe_2O_3 content appear reddish and this can be considered as a deficiency for kaolin application.

The average content of Fe_2O_3 in the studied samples is 2.3 wt.% while the pure kaolin samples (K05, K07, and K06) show 0.32, 0.17, and 0.06 wt.% Fe_2O_3 contents, respectively. Low Fe_2O_3 contents can be considered as an advantage for Kejal kaolin applications.

The concentration variations during hydrothermal alteration and the kaolinization process have been evaluated by many researchers using different methods. The immobile elements method (Nesbitt, 1979; MacLean and Kranidiotis, 1987; MacLean, 1990; Nesbitt and Markovics, 1997), isocon method (Baumgartner and Olsen, 1995; Grant, 2005), and volume factor method (Gresens, 1967) are the most popular tools in this regard. In the present study, we applied the immobile elements method to evaluate elemental changes during the kaolinization process. Among the immobile elements (Al, Ti, Zr, and Y), Ti shows the least mobility in the Kejal kaolinization profile (Figure 9a). Thus, Ti was chosen as an index element and the variation of the other constituents was calculated based on Ti values. Due to the decomposition of Ti-bearing minerals such as ilmenite and pyroxene, this element can be released to the hydrothermal system and, in some cases, Ti establishes itself in the structure of anatase and rutile. Augite usually contains 0.5%0.8 wt.% TiO_2 (Deer et al., 1992; Abedini et al., 2015).

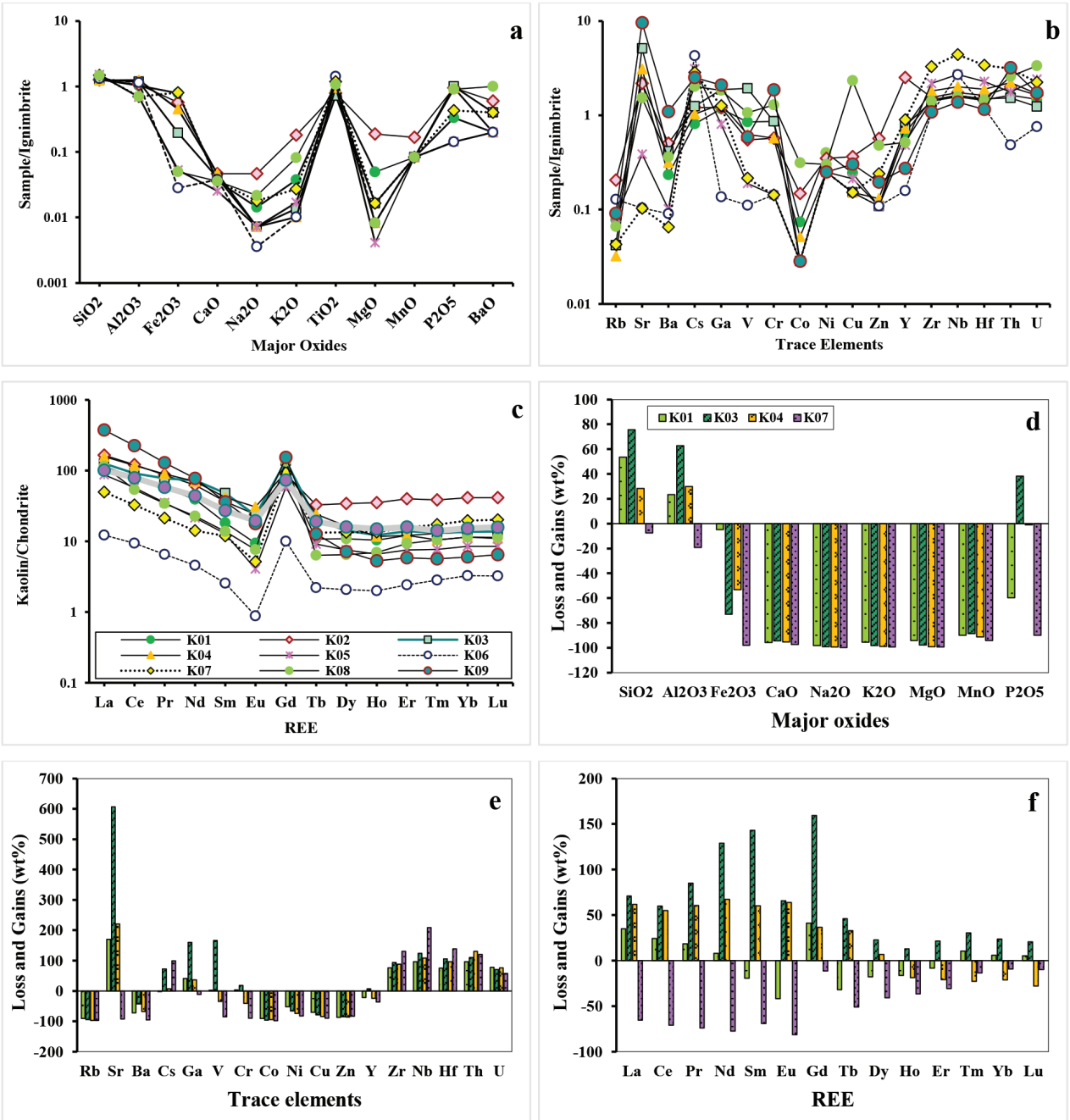

Figure 9. The elemental variation patterns and mass change values in the studied samples. a) Major oxides normalized to the ignimbritic parent rock; b, c, and d) the mass change values for major oxides, trace elements, and REEs respectively; e) REE patterns normalized to chondrite; f) trace elements normalized to the ignimbritic parent rock.

Mass change calculation is one of the most important evaluation methods in the alteration environment. The result of mass change calculations based on Ti concentrations is presented in Table 4 and the mass change values are plotted in Figures 9b, 9c, and 9d (only for the samples K01, K03, K04, and K07). The presented data were obtained using the formula proposed by Nesbitt (1979):

$$\text{Variation (\%)} = [((\text{Element}_{\text{Kaolin}} / \text{TiO}_{2\ \text{Kaolin}}) / (\text{Element}_{\text{Ignimbrite}} / \text{TiO}_{2\ \text{Ignimbrite}})) - 1] \times 100$$

The mass change calculations of the selected samples (Figures 9b, 9c, and 9d) reveal high enrichments for SiO_2 and Al_2O_3 during kaolinization (Figure 9b). Furthermore, P_2O_5 is also relatively enriched. The variation of P_2O_5 concentrations can be considered due to apatite dissolution

Table 4. The result of mass change calculations for Kejal kaolin samples based on Ti immobile element using formula proposed by Nesbitt (1979).

Sample		SiO_2	Al_2O_3	Fe_2O_3	CaO	Na_2O	K_2O	TiO_2	MgO	MnO	P_2O_5	La	Ce
Semialtered	K01	53.62	23.38	–4.69	–95.68	–98.27	–95.50	0.00	–94.07	–89.95	–59.79	35.15	24.37
Semialtered	K02	60.13	35.30	–27.98	–94.13	–94.10	–77.24	0.00	–76.12	–78.89	20.63	106.56	95.35
Semialtered	K03	75.71	62.86	–73.05	–94.47	–99.01	–98.13	0.00	–97.73	–88.48	38.18	70.86	59.84
Semialtered	K04	28.37	29.80	–53.19	–95.18	–99.25	–98.94	0.00	–99.15	–91.32	–0.85	61.56	54.98
Fully altered	K05	32.96	–39.17	–95.33	–97.77	–99.37	–98.50	0.00	–99.64	–92.64	–87.38	–23.73	–35.68
Fully altered	K06	33.59	–92.10	–99.25	–98.24	–98.09	–98.20	0.00	–99.69	–93.67	–92.76	–90.85	–90.91
Semialtered	K07	–7.55	–19.12	–98.02	–97.33	–99.75	–99.28	0.00	–99.42	–94.14	–89.95	–65.54	–70.84
Semialtered	K08	25.19	–74.45	12.36	–96.98	–98.49	–97.71	0.00	–98.62	–92.96	–63.81	–4.69	–42.19
Fully altered	K09	36.69	–34.20	–95.35	–96.64	–97.98	–92.37	0.00	–99.23	–92.18	127.87	246.89	166.97
Sample		Pr	Nd	Sm	Eu	Gd	Tb	Dy	Ho	Er	Tm	Yb	Lu
Semialtered	K01	18.40	8.03	–19.38	–41.88	41.15	–31.82	–17.73	–16.14	–8.22	10.29	5.92	5.17
Semialtered	K02	88.59	80.86	70.25	55.45	52.52	116.62	172.67	196.59	218.41	243.81	243.44	231.28
Semialtered	K03	85.01	128.93	143.19	65.82	159.44	46.19	22.71	12.90	21.38	30.29	23.58	20.47
Semialtered	K04	60.41	67.30	60.29	63.74	36.69	32.78	6.76	–18.74	–20.80	–22.66	–21.28	–27.92
Fully altered	K05	–46.65	–56.47	–58.44	–81.52	–29.06	–57.74	–57.95	–61.20	–58.07	–52.03	–50.78	–52.42
Fully altered	K06	–91.41	–92.06	–92.85	–96.55	–89.66	–91.19	–90.14	–89.80	–88.38	–84.80	–83.63	–84.41
Semialtered	K07	–74.07	–77.24	–69.17	–81.45	–11.44	–51.05	–40.73	–36.50	–30.73	–13.54	–9.32	–9.78
Semialtered	K08	–50.12	–56.31	–57.36	–66.99	55.10	–71.85	–65.84	–60.87	–50.33	–37.27	–36.50	–39.37
Fully altered	K09	109.37	65.71	24.48	–14.70	95.95	–37.45	–57.98	–66.82	–65.41	–62.47	–63.00	–61.51
Sample		Rb	Sr	Ba	Cs	Ga	V	Cr	Co	Ni	Cu	Zn	Y
Semialtered	K01	–90.59	170.27	–71.94	–2.69	41.15	2.50	3.40	–91.09	–51.75	–70.76	–86.89	–21.35
Semialtered	K02	–74.02	176.47	–35.93	52.84	52.52	–30.46	–27.62	–81.29	–55.67	–53.94	–28.41	216.95
Semialtered	K03	–94.24	606.41	–42.67	72.27	159.44	166.43	18.44	–96.07	–65.45	–79.06	–84.98	6.53
Semialtered	K04	–96.66	220.67	–67.48	6.89	36.69	–34.68	–40.51	–94.68	–73.97	–84.23	–86.42	–24.78
Fully altered	K05	–92.73	–65.87	–91.04	174.54	–29.06	–83.25	–87.38	–97.49	–77.91	–81.25	–90.39	–57.57
Fully altered	K06	–90.26	–92.13	–93.13	225.28	–89.66	–91.56	–89.14	–97.84	–81.00	–88.48	–91.74	–87.95
Semialtered	K07	–96.99	–92.76	–95.42	99.38	–11.44	–84.82	–89.95	–98.00	–82.41	–89.34	–83.17	–36.76
Semialtered	K08	–94.41	29.10	–69.59	70.58	55.10	–10.59	8.57	–73.61	–74.67	97.04	–59.61	–56.48
Fully altered	K09	–91.48	799.18	2.36	135.19	95.95	–44.81	74.25	–97.33	–76.54	–71.57	–81.64	–74.37
Sample		Zr	Nb	Hf	Th	U	-	-	-	-	-	-	-
Semialtered	K01	75.68	96.69	75.04	96.48	77.78	-	-	-	-	-	-	-
Semialtered	K02	96.15	120.29	106.14	151.82	106.67	-	-	-	-	-	-	-
Semialtered	K03	93.19	124.30	105.92	110.17	70.58	-	-	-	-	-	-	-
Semialtered	K04	88.00	108.22	95.97	130.66	76.34	-	-	-	-	-	-	-
Fully altered	K05	92.62	138.86	101.00	56.11	112.26	-	-	-	-	-	-	-
Fully altered	K06	–20.31	103.77	–9.10	–63.14	–42.55	-	-	-	-	-	-	-
Semialtered	K07	130.58	208.51	138.71	119.96	57.24	-	-	-	-	-	-	-
Semialtered	K08	19.29	32.79	20.87	117.43	182.02	-	-	-	-	-	-	-
Fully altered	K09	2.03	29.18	8.55	198.90	61.62	-	-	-	-	-	-	-

and establishment. Most of the major oxides show depletion (Figure 9b), suggesting that most of the major elements have been removed from the environment. Each element shows different behaviors during kaolinization and these behaviors must be evaluated separately. The oxidation of pyrite along with sulfuric acid production plays a great role in removal and fixation of Fe throughout the kaolinization profile. Na, K, Ca, Rb, Ba, and Cs are mobile elements in alterations and the main source of these elements is decomposition of feldspars. The breakdown of ferromagnesian minerals under hydrothermal fluids causes liberation of Mg, Mn, Co, Ni, and Cu into the system and that is the reason for the negative anomaly for these elements in the kaolin samples (Arslan et al., 2006; Abedini and Calagari, 2015). Sr shows fluctuations with different patterns in the severely altered and slightly altered samples (Figures 9c and 9e).

In the samples with a medium grade of alteration, the concentration of Sr has maximum values (K01, K03, K04, K07, and K09). In these samples, the concentration of Sr is even greater than in the ignimbritic parent rock. The intensely altered samples show low concentration values for Sr (K05, K06, and K07).

High field-strength elements (HFSEs) including Nb, Ta, Hf, Zr, Th, and U show enrichment in the kaolin samples (Figures 9c and 9e). These elements are relatively immobile in many altered zones (Jiang et al., 2003), but under acidic pH, a high water/rock ratio, and the accessibility of CO_3^{2-}, F^-, Cl^-, PO_3^{4-}, and SO_4^{2-} complexes, the transportation and fixation of HFSEs varies greatly (Fulignati et al. 1999). Salvi and William-Jones (1996) believe that in high-temperature alterations, HFSEs tend to be mobile and Zr can exit the system, whereas in low-temperature systems HFSEs are usually immobile. In the Kejal alteration, the enrichment of HFSEs can be considered as a sign of a low-temperature hydrothermal system.

Although it is believed that REEs are resistant to mineral decomposition during alteration (Patino et al., 2003; Uysal and Golding, 2003; Karadağ et al., 2009), some researchers have proposed that REEs show different behaviors along weathering processes. In general, the composition and mineralogy of parent rock are of the utmost importance and control the mobility and distribution of REEs (MacLean et al., 1987; Hill et al., 2000; Hongbing et al., 2004).

Therefore, REEs can be released from primary minerals and adsorbed by secondary minerals (Karadağ et al., 2009). REEs have been investigated by many researchers (e.g., Clark, 1983; Fleischer and Altschuler, 1986; Fleischer, 1987; Solodov et al., 1987; Banifield and Eggleton, 1989; Burt, 1989; Condie, 1991; Braun et al., 1993; Miyawaki and Nakai, 1993; Koppi et al., 1996; Mutakyahwa et al., 2003; Pokrovsky et al., 2006; Ahmadnejad et al., 2017). These studies show secondary minerals such as Fe-Mn oxides and hydroxides, phosphates, and clay minerals. In general, the concentration of REEs depends on the mineral resistance against weathering. The resistant minerals are usually accumulated in the weathered profile, while the unstable minerals release their REE contents. The released REEs may be accumulated in the supergene zone (Middelburg et al., 1988).

The REE contents of studied samples are represented in Table 1. Figure 9f shows the REE values normalized to chondrite while Figure 9d shows REE mass changes in K01, K03, K04, and K07. Based on the obtained data (Table 5), the highest ΣREE belong to K02 and K09 (201.9 and 316.4 ppm, respectively). A brief look at the REE diagram (Figure 9f) reveals that the REE patterns follow relatively flat trends with a slight enrichment in the Ce group (LREE) relative to the Y group (HREE). The enrichment rate of LREEs/HREEs in the studied sample is 4:1. As a general statement, REEs tend to accumulate on clay minerals in cation form. Considering the low solubility of the Ce group compared to the Y group, LREEs can always accumulate in the upper parts of weathering profiles along with clay minerals (Nesbitt, 1979; Nesbitt and Wilson, 1992; Al-Ani and Sarapaa, 2009). LREE concentrations in the Kejal kaolinized horizon can be explained by this fact.

Eh and pH control REE mobility more than the other parameters. The relatively acidic environment during chemical weathering and kaolinization causes the removal of elements from the parent rock. The REE adsorption by clay minerals increases when pH rises. A pH range of 7–9 is the most suitable condition for the adsorption of REEs by clays. The presence of kaolinite as the main clay mineral in Kejal kaolin samples on the one hand and the REE concentrations on the other hand reveals the role

Table 5. The REE related parameters calculated for Kejal kaolin samples.

Sample ID		ΣREE	ΣLREE	ΣHREE	Eu/Eu*	Ce/Ce*
Semialtered	K01	129.23	103.34	25.89	0.44	0.99
Semialtered	K02	129.13	103.53	25.6	0.24	0.95
Semialtered	K03	201.93	157.62	44.31	0.42	0.97
Semialtered	K04	172.46	134.86	37.6	0.29	0.90
Fully altered	K05	187.35	158.17	29.18	0.48	0.95
Fully altered	K06	88.73	71.39	17.34	0.15	0.94
Semialtered	K07	15.61	11.84	3.77	0.17	1.01
Semialtered	K08	72.09	42.45	29.64	0.15	0.92
Fully altered	K09	109.55	76.46	33.09	0.18	0.73

of kaolinite in REE accumulation in these samples. As mentioned by Coppin et al. (2002), kaolinite adsorbs REEs from hydrous phases.

The positive correlation between Al_2O_3 and ΣREE (R^2 = 0.51) (Figure 10a) can be due to the adsorption by clay minerals (McBride, 1987). There is a good positive correlation between TiO_2 and ΣREE (Figure 10b), suggesting the role of Ti minerals like ilmenite, pyroxene, rutile, and anatase in REE establishment (Deer et al., 1992). On the other hand, the considerable percentage of P_2O_5 in some samples (Figure 9a) and the positive correlation between P_2O_5-ΣLREE (R^2 = 0.9) and P_2O_5-ΣREE (R^2 = 0.74) (Figures 10c and 10d) demonstrate the effect of some accessory REE-bearing minerals like monazite (Ce, La, Nd, Th) (PO_4,SiO_4) in REE attraction. In general, the comparison of REE diagrams for kaolin and the parent rock (Figure 9e) shows relatively similar patterns but different concentration values. Some samples show a high concentration of REEs relative to precursor rock and some others, especially K06, show values lower than that of precursor rock. Since K06, as an example of intensely altered rock, has experienced silicification, it chiefly contains SiO_2 while being depleted in other constituents.

Gd shows a marked positive anomaly (Figure 9f). Gd is classified as MREE or HREE. Gd has special properties and is applicable in different fields of study. During the 1980s, because of its paramagnetic properties, GD was used as a contrast agent in magnetic resonance imaging (MRI). This REE behaves like Ca^{2+} from a geochemical point of view (Rabiet et al., 2014). Many authors have reported Gd anomalies in surface and underground waters (Möller et al., 2000, 2002; Nozaki et al., 2000; Elbaz-Poulichet et al., 2002; Rabiet et al., 2005, 2009; Verplanck et al., 2005). Möller et al. (2011) reported that Gd complexes may be decomposed in the presence of some elements such as Cu, Y, and REEs with release of Gd^{3+} to the environment. Since Ca is one of the major elements in the composition of ignimbritic parent rock (in the structure of aluminosilicates such as plagioclase) in the Kejal area, the Gd anomaly in the Kejal kaolin is most likely related to the primary Ca content of the parent rock. Furthermore, the decomposition of Gd complexes in the presence of competitor elements or the high Gd content of hydrothermal fluids can be considered as other reasons for the positive Gd anomaly in kaolin samples.

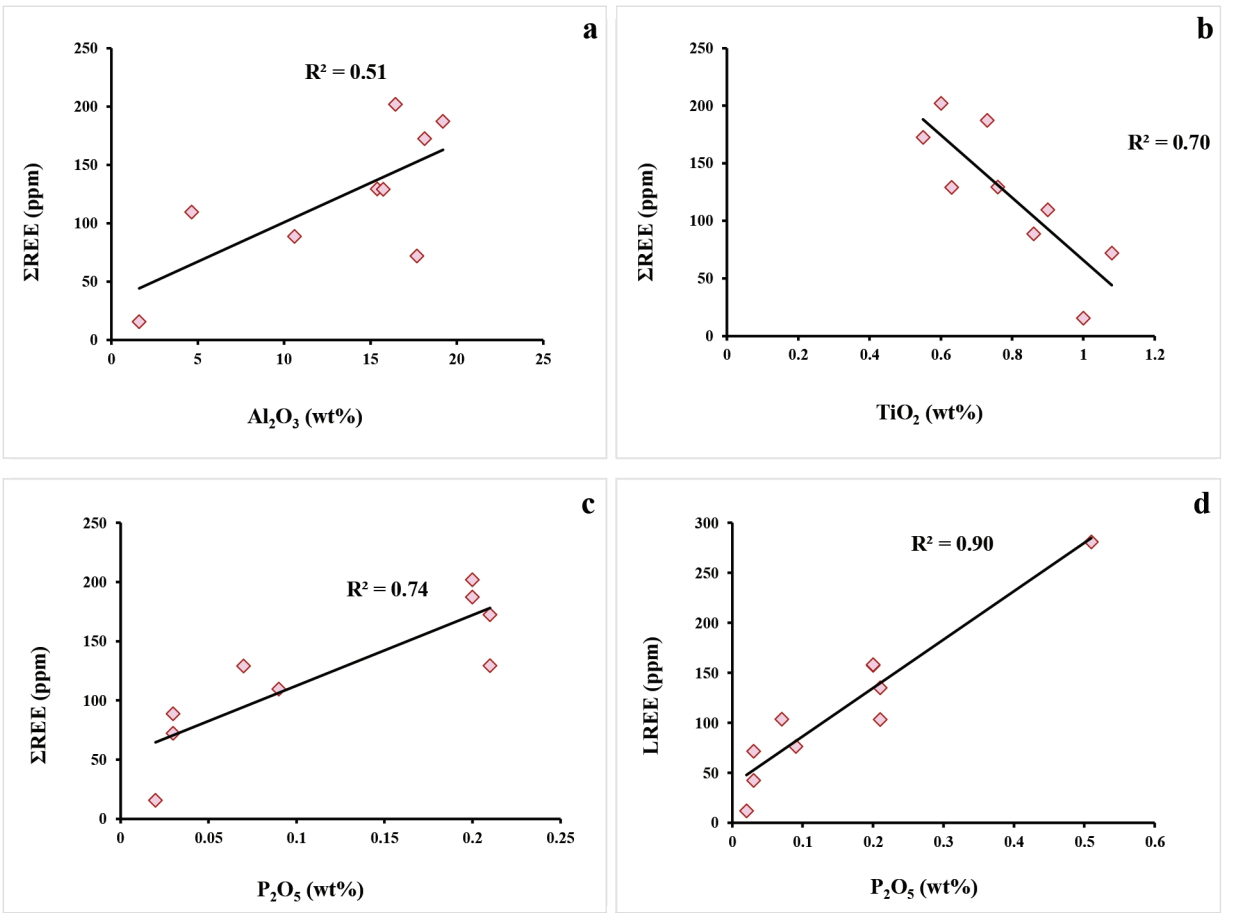

Figure 10. a–d) Bivariate diagrams showing the correlation between REEs and some major oxides.

Eu and Ce anomalies are suitable tools to interpret the geological and physicochemical conditions of the environment (De Baar et al., 1983; Braun et al., 1990; Bau, 1999; Davranche et al., 2005; Class and Le Roex, 2008; Leybourne and Johannesson, 2008; Mameli et al., 2008; Seto and Akagi, 2008; Kerrich and Said, 2011; Chetty and Gutzmer, 2012; Mongelli et al., 2014). In the current study, we used the formula proposed by Taylor and McLennan (1985):

$Eu/Eu^{*} = Eu_N/[(Sm_N \times Gd_N)]^{1/2}$, $Ce/Ce^{*} = 2Ce_N/(La_N + Pr_N)$

Here, Eu and Ce represent europium and cerium and Eu_N, Sm_N, Gd_N, Ce_N, La_N, and Pr_N represent normalized europium, samarium, gadolinium, cerium, lanthanum, and praseodymium, respectively.

The Eu patterns on the REE diagram normalized to chondrite show slight depletion (Figure 9f). Table 5 represents the results of Eu/Eu^{*} calculations for the studied samples, which change between 0.15 and 0.48. As mentioned in the previous sections, most rock units in the Kejal area have been subjected to severe alterations. Furthermore, as Eu has a high concentration in the composition of Ca-plagioclase, during the kaolinization and the alteration of feldspars to clay minerals under high temperatures and redox conditions, Eu^{3+} changes to Eu^{2+} and leaves the system. The negative Eu anomaly in the Kejal kaolins could be due to this process. On the other hand, the oxidation of pyrite and the formation of fluids of an acidic nature can also cause such a negative anomaly.

Among REEs, Ce with high ionic potential has a different behavior (McLennan, 1989). Ce and La show high values compared to the other REEs in the study area. Ce can be naturally found in the forms of Ce^{3+} and Ce^{4+}. Ce is usually accumulated in oxidant environments and upper parts of the weathering profile in the form of Ce^{4+} (Braun et al., 1990; Mongelli, 1997; Ji et al., 2004; Mameli et al., 2008; Wang et al., 2013; Mongelli et al., 2014; Zamanian et al., 2016). As can be seen from Table 5, Ce/Ce^{*} ratios range between 0.73 and 1.01 in the Kejal kaolins. These values represent a positive anomaly that can be produced under oxidizing conditions.

5.2. Application potentials

The feasibility study of kaolin applications in industrial affairs makes it possible to use this nonmetallic material appropriately. Kaolin has traditional and technological uses in different industries such as paper, ceramic, paint, abrasive, and plastic industries. Therefore, the first step in determining the final consumption is the study of the physicochemical properties of kaolin samples. Here we have evaluated the physicochemical characteristics of the Kejal kaolin deposit and compared it with the present industrial standards.

5.2.1. Paper industry

Kaolin is the main white material used in the paper industry for filler and coating purposes. As filler, its function is related to the internal network of the paper, whereas as coating it enhances the surficial properties of paper, such as brightness, smoothness, glossiness, and ink receptivity.

The analysis of grain size distribution in kaolin deposits is a very important step in the evaluation of kaolin for industrial uses. The reason is that the grain size of kaolin particles affects the quality of kaolin's final products; hence, fine particles (<2 μm) are the most desirable.

Since finer kaolinite particles have improved brightness and gloss characteristics and superior hiding power, coating grades are much finer than filler grades, with typically >75% of 2 μm particles compared to >30% of 2 μm for filler grades (Table 6).

As seen in Table 2, the frequency of <2 μm particles in the studied samples is almost 20% and that of particles greater than 10 μm (10–25 μm) is about 30%. These distribution ranges represent the dominant frequency of medium sizes. Therefore, the use of the studied kaolin samples is not recommended for coating purposes, but the results of particle size testing are close to the values needed for filler applications and under special circumstances these kaolins can be used as filler.

The use of kaolin in the paper industry is dependent on particle size rather than other parameters. However, the other characteristics are still important. Among these characteristics, the chemical composition of kaolin is worth noting. Different chemical compositions may cause special colors. For example, the high iron oxide content of kaolin samples may cause a red color, which is considered as a deficiency for use as a white raw material. Regarding the low iron content of the fully altered (pure) kaolin in the study area (K05 = 0.32, K06 = 0.06, and K07 = 0.17 wt.%), these kaolin samples possess enough whiteness, and if the other parameters are suitable, this kaolin can be used in the paper industry.

5.2.2. Ceramic industry

Clay is an essential raw material in ceramic products, composing 25%–100% of the ceramic body. Kaolin is one of a number of clays used in this industry. Kaolin makes up an average of 25% of earthenware, 60% of porcelain, 20%–30% of vitreous-china sanitary ware, and 20% of electrical porcelain and wall tiles (Jepson, 1984).

In general, the kaolin used in ceramic industry requires high Al_2O_3 content. Table 6 represents the chemical composition of kaolin used in some products in the ceramic industry. As seen in Table 6, products such as super standard porcelain and sanitary ware should have high alumina contents and therefore only kaolins with

Table 6. Physical and chemical parameters required for kaolin applications. The required particle size values for paper industry from Bloodworth et al. (1993) and the chemical composition of kaolin used in some products of ceramic industry from Bloodworth et al. (1993) and Fatahi et al. (2017) and KK1 from Kejal kaolin.

Physical parameters											
Particle size		Filler (%)			Coating (%)			Studied kaolin (KK1) (%)			
<2 μm		25–60			75–95			~20			
>10 μm		6–25			0–6			~30			
Chemical parameters											
Applications	Applications	Chemical Composition (wt%)									
		SiO_2	TiO_2	Al_2O_3	Fe_2O_3	CaO	MgO	K_2O	Na_2O	P_2O_5	LOI
	Super standard porcelain	47	0.03	38	0.39	0.1	0.22	0.8	0.15	-	13
	Sanitary ware	48	0.05	37	1	0.07	0.3	2	0.1	-	7.5
	Ceramic floor tiles	60–68	0.4	14	1	1–2	0.7–1	3–4	0.5	1	5–7
	Chinese ceramic	47.9	0.03	37.2	0.68	0.08	0.2	1.39	0.08	-	12.7
	Studied kaolin (KK1)	69.3	0.55	18.15	1.18	0.19	0.04	0.04	0.02	0.21	8.2

high Al_2O_3 contents are used as raw materials for these purposes. On the other hand, the silica content of this raw material should be less than 50% in super standard porcelain and sanitary ware products.

Low-grade kaolin is usable for different purposes after processing. For example, dry or wet dressing of raw kaolin composed of SiO_2 (up to 70%), Al_2O_3 (up to 22%), Fe_2O_3 (up to 1.5%), and CaO + MgO + alkalis (up to 3%) and characterized by refractoriness of about 1530 °C would yield white kaolin concentrate containing 46.07% to 46.85% SiO_2, 31.78% to 39.83% Al_2O_3, 0.30% to 0.73% Fe_2O_3, 0.25% to 0.35% TiO_2, and 0.15% to 0.56% CaO with LOI of 13.34% to 13.97%. The refractoriness of the concentrate would be about 1690 °C, with its white color index ranging from 65% to 88% (Sabov et al., 1985).

The alumina and silica contents of the studied kaolin samples are slightly different from the required composition for super standard porcelain and sanitary ware products, but these kaolins are applicable in other products such as ceramic floor tiles. Furthermore, after processing, this kaolin can be used for other aims.

Particle size is also important in order to identify the application possibilities of kaolin in the ceramic industry. In high-quality ceramics like super standard porcelain, more than 85% of the grains should be <2 μm, whereas in some products such as floor tiles there is no need for high percentages of <2 μm particles.

In both the ceramic and the paper industries, the main reason for the use of kaolin is its particular properties such as high brightness, low abrasiveness, and small particle size. The relatively low cost of kaolin, while being an important factor, is not nearly as important as the physical characteristics of the mineral. In the applications discussed in this section and also other cases such as rubber and paint, the lower cost of kaolin and its physical properties are important.

5.2.3. REE extraction potential

With regard to industrial and technological advancement in recent years, the demand for REEs has greatly increased and less conventional sources of REEs are being explored for economic viability. Over the past years, four primary types of deposits have been known for containing REEs (Van Gosen, 2014). These deposits include carbonatites, alkaline igneous rocks, ion-adsorption clays, and monazite-xenotime-bearing placer deposits (Van Gosen, 2014). Recent studies, however, suggest the potential of REE extraction from alternative sources such as coal, ocean water, and regoliths associated with coastal plain clays (Foley and Ayuso, 2015; Drost and Wang, 2016; Rozelle et al., 2016). Gardner (2016) studied the REE contents of Georgian kaolins and evaluated the exploration potentials of this deposit. He found some REE-bearing minerals such as zircon and monazite, which contain considerable amount of REEs.

The REEs in kaolin samples can be due to absorption of these elements by kaolinite. Kaolinite flakes absorb a large part of the released Ce, La, and Nd during kaolinization and weathering (Papoulis et al., 2004).

ΣREE values of kaolinized samples were calculated for Kejal kaolin and are presented in Table 5. The highest ΣREE is that of K03 (201.93 ppm). Although the concentrations of REEs in Kejal kaolin samples are considerable, these REE contents are not close to economic grades. Based on the XRD analyses, there is no sign of REE-bearing minerals such as monazite or zircon in the studied samples. The absorption of REEs by clays is most likely the main agent of REE concentration.

6. Conclusions

Upon the evaluation of geological and geochemical characteristics of the Kejal kaolin deposit, we obtained the following results:

- From a geological point of view, the Kejal kaolin deposit is located in an alteration zone that has experienced medium to advanced grades of argillic alterations. The kaolin product in this area is observable in a white to red spectrum of colors. The parent rock of kaolin is ignimbrite, and volcanic tuff and kaolinization intensely occur along faults and fractures. At some points, silicification has a remarkable outcrop, which has considerably reduced the quality of kaolin.

- Based on XRD analysis, kaolinite is the main clay mineral in the studied samples. Quartz and cristobalite consist of the silica minerals of the deposit, and anatase is found in trace amounts in some parts.

- Major oxides follow the distribution order of SiO_2 > Al_2O_3 > Fe_2O_3 > TiO_2 > CaO > P_2O_5 > K_2O > Na_2O > MgO > MnO in the pure kaolin. The maximum Al_2O_3 and TiO_2 contents in the samples are 19.2% and 1.08%, respectively. SiO_2 has been highly concentrated in most of the samples and shows 73% on average. It seems that the replacement of Al with Si occurred in kaolins and increased the SiO_2 content of the samples; nevertheless, there is a possibility of Al removal due to high water/rock ratios.

- The mass change calculations considering TiO_2 as an immobile monitor element show the enrichment of Si, Al, P, Sr, Ga, Nb, Zr, Hf, Th, U, La, Ce, Nd, and Gd and depletion of Fe, Na, K, Ca, Mg, Mn, Cu, Ni, and Zn during the kaolinization process.

- The REE contents of studied samples normalized to chondrite show similar patterns. There is an enrichment in LREEs compared with HREEs. The Gd positive anomaly and Eu negative anomaly are also observable. LREE enrichment can be due to low solubility potentials of these rare elements. The Gd positive anomaly is most likely caused by the decomposition of Gd complexes in the presence of competitor elements such as Cu, Y, and REEs. The similar behavior of Gd and Ca and the abundance of Ca in the ignimbritic parent rock can be another reason for the positive anomaly of Gd.

- The bivariate plots of REEs and major oxides show good positive correlations between TiO_2-ΣREE (R^2 = 0.7), Al_2O_3-ΣREE (R^2 = 0.51), P_2O_5-ΣLREE (R^2 = 0.9), and P_2O_5-ΣREE (R^2 = 0.74). It is implied that clay minerals such as kaolinite, Ti-bearing minerals like rutile and anatase, and REE-bearing phosphate minerals such as monazite have played an important role in the concentration and establishment of REEs during Kejal kaolinization.

- The negative Eu anomaly in the studied samples is related to the alteration of feldspars and the formation of clay minerals. This process has removed Eu^{2+} from the environment and caused the negative Eu anomaly. The Ce positive anomaly could be due to the oxidation of Ce^{3+} to Ce^{4+} and the concentration of Ce in the system.

- The particle size test carried out based on a hydrometer test for the Kejal kaolin samples reveals particle size distribution patterns in which medium-sized particles (10–25 μm) are dominant (30%) and the frequency of <2 μm particles is almost 20%.

- Some other physical properties of Kejal kaolin were measured and calculated including specific gravity (2.45–2.62), moisture content (0.379%–0.866%), natural weights and dry and saturated weights (42.16–80.81, 42–89.8, and 58.6–89.8), and viscosity (37.9–39.3 P). Among these properties, the viscosity of kaolin pulp is an important parameter and the low viscosity of the studied samples reveals a suitable viscosity level for the paper industry.

- The medium particle size, high silica content, and intermediate alumina content of the Kejal kaolin deposit indicate that although this kaolin is not applicable for several special purposes such as super standard porcelain and sanitary ware in the ceramic industry or coatings in the paper industry, this kaolin can be used after simple processing in floor tile manufacturing and as a filler material in the paper industry.

- The REE concentrations in the studied samples represent considerable values. Even though these concentrations are worth noting, these concentrations are not comparable with REE economic sources. The lack of REE-bearing minerals such as monazite and zircon can be thought of as a reason for the relatively low concentration.

Acknowledgment

This study was supported financially and logistically by Mohaghegh Ardabili University and the University of Tabriz. The authors would like to thank all the staff members of these universities for their generous support.

References

Abedini A, Alipour S, Khosravi M (2015). Investigation of mineralogy, geochemistry and industrial applications of Darzi-vali bauxite ores, east of Bukan, NW Iran. Scientific Quarterly Journal of Geosciences 24 (94): 293-304 (in Persian).

Abedini A, Calagari AA (2015). Geochemical characteristics of the Abgharm kaolin deposit, NW Iran. Neues Jahrbuch für Mineralogie Abhandlugen 278 (3): 125-139.

Abedini A, Masoumi R, Calagari AA (2011). Geochemical features of Kejal kaolin deposit, NW Hashtjin, Ardabil province. Journal of Economic Geology 2 (3): 165-181 (in Persian).

Aghanabati A (2004). Geology of Iran. 1st ed. Tehran, Iran: Geological Survey of Iran (in Persian).

Ahmadnejad F, Zamanian H, Taghipour B, Zarasvandi A, Buccione R et al. (2017). Mineralogical and geochemical evolution of the Bidgol bauxite deposit, Zagros Mountain Belt, Iran: implications for ore genesis, rare earth elements fractionation and parental affinity. Ore Geology Reviews 86: 755-783.

Al-Ani T, Sarapää O, Juhanson B (2009). Concentration and Residence of Rare Earth Elements (REE) in Kaolin and Weathered Rock of Virtasalmi, Taivalkoski and Puolanka Deposits, in Eastern Finland. GTK Internal Report. Helsinki, Finland: Geological Survey of Finland.

Alavi M (1996). Tectonostratigraphic synthesis and structural style of the Alborz Mountains system northern Iran. Journal of Geodynamics 21 (1): 1- 33.

Aref AA, Lei XR (2009). Characterization and evaluation of Algaof kaolin deposits of Yemen for industrial application. American Journal of Engineering and Applied Sciences 2 (2): 292-296.

Arslan M, Kadir S, Abdioglu E, Kolayli H (2006). Origin and formation of kaolin minerals in saprolite of Tertiary alkaline volcanic rocks, Eastern Pontides, NE Turkey. Clay Minerals 41 (2): 597-617.

ASTM (1998). D422-63. Standard Test Method for Particle-Size Analysis of Soils. West Conshohocken, PA, USA: ASTM International.

Banifield JF, Eggleton RA (1989). Apatite replacement and REE mobilization, fractionation, and fixation during weathering. Clays and Clay Minerals 37 (2): 113–127.

Bau M (1999). Scavenging of dissolved yttrium and rare earths by precipitating iron oxyhydroxide: experimental evidence for Ce oxidation, Y-Ho fractionation, and lanthanide tetrad effect. Geochimica et Cosmochimica Acta 63 (1): 67-77.

Baumgartner LP, Olsen SN (1995). A least-squares approach to mass transport calculations using the Isocon method. Economic Geology 90 (5): 1261-1270.

Beazley KM (1972). Viscosity-concentration relations: in deflocculated kaolin suspensions. Journal of Colloid and Interface Science 41 (1): 105-115.

Bloodworth AJ, Highley DE, Mitchell CJ (1993). Industrial Mineral Laboratory Manual: Kaolin. Nottingham, UK: British Geological Survey.

Braun JJ, Pagel M, Herbillon A, Rosin C (1993). Mobilization and redistribution of REEs and thorium in a syenitic lateritic profile: a mass balance study. Geochimica et Cosmochimica Acta 57 (18): 4419-4434.

Braun JJ, Pagel M, Muller JP, Bilong P, Michard A et al. (1990). Cerium anomalies in lateritic profiles. Geochimica et Cosmochimica Acta 54 (3): 781-795

Bundy WM (1993). The diverse industrial applications of kaolin. In: Murray HH, Bundy W, Harvey C (editors). Kaolin, Genesis, and Utilization. Special Publication 1. Boulder, Colorado, USA: The Clay Minerals Society, pp. 43-73.

Burt DM (1989). Compositional and phase relations among rare earth element minerals. In: Lipin BR, McKay GA (editors). Geochemistry and Mineralogy of Rare Earth Elements. Washington, DC, USA: The Mineralogical Society of America, pp. 259-307.

Chetty D, Gutzmer J (2012). REE redistribution during hydrothermal alteration of ores of the Kalahari manganese deposit. Ore Geology Reviews 47: 126-135.

Clark AM (1983). Mineralogy of the rare earth elements. In: Henderson P (editor). Rare Earth Element Geochemistry. 1st ed. Amsterdam, the Netherlands: Elsevier, pp. 33-61.

Class C, le Roex AP (2008). Ce anomalies in Gough Island lavas - Trace element characteristics of a recycled sediment component. Earth and Planetary Science Letters 265 (3-4): 475-486.

Condie KC (1991). Another look at rare-earth elements in shales. Geochimica et Cosmochimica Acta 55 (9): 2527-2531.

Coppin F, Berger G, Bauer A, Castet S, Loubet M (2002). Sorption of lanthanides on smectite and kaolinite. Chemical Geology 182 (1): 57-68.

Cravero F, Gonzales I, Galan E, Dominguez E (1997). Geology, mineralogy, origin and possible applications of some Argentinian kaolins in the Neuquen basin. Applied Clay Science 12 (1-2): 27-42.

Çelik H (2010). Technological characterization and industrial application of two Turkish clays for the ceramic industry. Applied Clay Science 50 (2): 245-254.

Davranche M, Pourret O, Gruau G, Dia A, Le Coz-Bouhnik M (2005). Adsorption of REE (III) humate complexes onto MnO_2: experimental evidence for cerium anomaly and lanthanide tetrad effect suppression. Geochimica et Cosmochimica Acta 69 (20): 4825-4835.

De Baar HJW, Bacon MP, Brewer PG (1983). Rare earth distributions with a positive Ce anomaly in the Western North Atlantic Ocean. Nature 301: 324-332.

Deer WA, Howie RA, Zussmann J (1992). An Introduction to the Rock-Forming Minerals. 2nd ed. New York, NY, USA: Wiley.

De Noni JA, Garcia DE, Hotza D (2002). A modified model for the viscosity of ceramic suspensions. Ceramics International 28 (7): 731-735.

Elbaz-Poulichet F, Seidel JL, Othoniel C (2002). Occurrence of an anthropogenic gadolinium anomaly in river and coastal waters of Southern France. Water Research 36 (4): 1102-1105.

Faridi M, Anvari A (2000). Geological Map of Hashtjin (1:100,000). Sheet 5664. Tehran, Iran: Geological Survey of Iran.

Fatahi S, Calagari AA, Abedini A, Tabatabaie SH, Mansouri Isfehani M (2017). Mineralogy, technological properties, and industrial application of kaolin deposits at Nivasht and Kabudkamar areas, northwest of Saveh, Central Province. Iranian Journal of Crystallography and Mineralogy 25 (3): 619-628 (in Persian).

Fleischer M (1987). Glossary of Mineral Species. 5th ed. Tucson, AZ, USA: Mineralogical Record.

Fleischer M, Altschuler ZS (1986). The lanthanides and yttrium in minerals of the apatite group - An analysis of the available data. Neues Jahrbuch für Mineralogie-Monatshefte 10: 467-480.

Fulignati P, Gioncada A, Sbrana A (1999). Rare earth element (REE) behaviour in the alteration facies of the active magmatic-hydrothermal system of Vulcano (Aeolian Islands, Italy). Volcanology and Geothermal Research 88 (4): 325-342.

Galán E, Aparicio P, Fernández-Caliani JC, Miras A, Márquez MG et al. (2016). New insights on mineralogy and genesis of kaolin deposits: the Burela kaolin deposit (Northwestern Spain). Applied Clay Science 131: 14-26.

Grant JA (2005). Isocon analysis: a brief review of the method and applications. Physics and Chemistry of the Earth 30 (17-18): 997-1004.

Gresens RL (1967). Composition-volume relationships of metasomatism. Chemical Geology 2: 47-65.

Hajalilou B (1999). Tertiary metallogeny in western Alborz-Azerbaijan (Mianeh-Siahroud) focused on Hashtjin area. PhD, Shahid Beheshti University, Tehran, Iran (in Persian).

Heinskanen K (1996). Particle Classification. 1st ed. London, UK: Chapman and Hall.

Hill IG, Worden RH, Meighan IG (2000). Geochemical evolution of a palaeolaterite: the Interbasaltic Formation, Northern Ireland. Chemical Geology 166 (1-2): 65-84.

Hongbing J, Wang S, Ouyang Z, Zhang S, Sun C et al. (2004). Geochemistry of red residua underlying dolomites in karst terrains of Yunnan-Guizhou Plateau. The formation of the Pingba profile. Chemical Geology 203 (1-2): 1-27.

Jepson WB (1984). Kaolins: their properties and uses. Philosophical Transactions of the Royal Society A: Mathematical, Physical and Engineering Sciences 311 (1517): 411-432.

Jiang N, Sun S, Chu X, Mizuta T, Ishiyama D (2003). Mobilization and enrichment of high-field strength elements during late- and post-magmatic processes in the Shuiquangou syenitic complex, Northern China. Chemical Geology 200 (1-2): 117-128.

Jiménez-Millán J, Abad I, Nieto F (2008). Contrasting alteration processes in hydrothermally altered dolerites from the Betic Cordillera, Spain. Clay Minerals 43 (2): 267-280.

Karadağ MM, Küpeli Ş, Arık F, Ayhan A, Zedef V et al. (2009). Rare earth element (REE) geochemistry and genetic implications of the Mortas bauxite deposit (Seydisehir/Konya-Southern Turkey). Chemie Der Erde-Geochemistry 69 (2): 143-159.

Kerrich R, Said N (2011). Extreme positive Ce-anomalies in a 3.0 Ga submarine volcanic sequence, Murchison Province: oxygenated marine bottom waters. Chemical Geology 280 (1-2): 232-241.

Koppi AJ, Edis R, Field DJ, Geering HR, Klessa DA et al. (1996). REEs trends and Ce\U\Mn associations in weathered rock from Koongarra, northern territory, Australia. Geochimica et Cosmochimica Acta 60 (10): 1695-1707.

Kuşcu M, Yıldız A (2016). The mineralogy, geochemistry, and suitability for ceramic applications of Akharım (Afyonkarahisar, W Turkey) kaolinitic clay. Arabian Journal of Geosciences 9 (7): 510.

Leybourne MI, Johannesson KH (2008). Rare earth elements (REE) and yttrium in stream waters, stream sediments, and Fe–Mn oxyhydroxides: fractionation, speciation, and controls over REE + Y patterns in the surface environment. Geochimica et Cosmochimica Acta 72 (24): 5962-5983.

Ligas P, Uras I, Dondi M, Marsigli M (1997). Kaolinitic materials from Romana (north-west Sardinia, Italy) and their ceramic properties. Applied Clay Science 12 (1-2): 145-163.

MacLean WH (1990). Mass change calculations in altered rock series. Mineralium Deposita 25 (1): 44-49.

MacLean WH, Kranidiotis P (1987). Immobile elements as monitors of mass transport in hydrothermal alteration: Phelps Dodge massive sulfde deposit, Matagami. Economic Geology 82 (4): 951-962.

Mahjoor AS, Karimi M, Rastegarlari A (2009). Mineralogical and geochemical characteristics of clay deposits from South Abarkouh district of clay deposit (Central Iran) and their applications. Journal of Applied Sciences 9 (4): 601-614.

Mameli P, Mongelli G, Oggiano G, Sinisi R (2008). Fe concentration in palaeosols and in clayey marine sediments: two case studies in the Variscan basement of Sardinia (Italy). Clay Minerals 43 (4): 531-547.

Manju CS (2002). Mineralogical, morphological and geochemical studies on Kundara and Madayi kaolins, Kerala. PhD, University of Kerala, Kerala, India.

Masoumi R (2010). Investigation of mineralogy and geochemistry of kaolin deposit in Kejal area, northwest of Hastjin, Ardebil province. MSc, University of Tabriz, Tabriz, Iran (in Persian).

McBride MB (1987). Chemistry of clays and clay minerals. Clays and Clay Minerals 36 (5): 480.

McLennan SM (1989). Rare earth elements in sedimentary rocks: influence of provenance and sedimentary processes. In: Lipin BR, McKay GA (editors). Geochemistry and Mineralogy of Rare Earth Elements. 1st ed. Washington, DC, USA: Mineralogical Society of America, pp. 169-200.

Middelburg JJ, van der Weijden CH, Woittiez JRW (1988). Chemical processes affecting the mobility of major, minor and trace elements during the weathering of granitic rocks. Chemical Geology 68 (3-4): 253-273.

Miyawaki R, Nakai I (1993). Crystal structures of rare-earth minerals. In: Gschneidner KA, Eyring L (editors). Handbook on the Physics and Chemistry of Rare Earths, 16. Amsterdam, the Netherlands: Elsevier, pp. 249-518.

Moayed M (2001). The investigation of Tertiary volcano-plutonic belt of Western Alberz-Azerbaijan (Mianeh-Siahroud) with a special regard to Hashtjin area. PhD, Shahid Beheshti University, Tehran, Iran (in Persian).

Moghadami I (2011). Geochemical investigations of Zeolitic alteration in volcanic rocks of Kejal area (Northwest of Hashtjin, Ardabil province). MSc, University of Tabriz, Tabriz, Iran (in Persian).

Möller P, Dulsky P, Bau M, Knappe A, Pekdeger A et al. (2000). Anthropogenic gadolinium as a conservative tracer in hydrology. Journal of Geochemical Exploration 69-70: 409-414.

Möller P, Knappe A, Dulski P, Pekdeger A (2011). Behavior of Gd-DTPA in simulated bank filtration. Applied Geochemistry 26 (1): 140-149.

Möller P, Paces T, Dulsky P, Morteani G (2002). Anthropogenic Gd in surface water, drainage system, and the water supply of the city of Prague, Czech Republic. Environmental Science & Technology 36 (11): 2387-2394.

Mongelli G (1997). Ce-anomalies in the textural components of Upper Cretaceous karst bauxites from the Apulian carbonate platform (southern Italy). Chemical Geology 140 (1-2): 69-79.

Mongelli G, Boni M, Buccione R, Sinisi R (2014). Geochemistry of the Apulian karst bauxites (southern Italy): Chemical fractionation and parental affinities. Ore Geology Reviews 63: 9-21.

Murray HH (1991). Overview: Clay mineral application. Applied Clay Science 5 (5-6): 379-395.

Murray HH, Keller WD (1993). Kaolins, kaolins, kaolins. In: Murray HH, Bundy WM, Harvey CC (editors). Kaolin Genesis and Utilization. Special Publication No. 1. Boulder, CO, USA: The Clay Minerals Society, pp. 1-24.

Mutakyahwa MKD, Ikingura JR, Mruma AH (2003). Geology and geochemistry of bauxite deposits in Lushoto District, Usambara Mountains, Tanzania. Journal of African Earth Sciences 36 (4): 357-369.

Nesbitt HW (1979). Mobility and fractionation of rare elements during weathering of a granodiorite. Nature 279: 206-210.

Nesbitt HW, Markovics G (1997). Weathering of granodioritic crust, long-term storage of elements in weathering profiles, and petrogenesis of siliciclastic sediments. Geochimica et Cosmochimica Acta 61 (8): 1653-1670.

Nesbitt HW, Wilson RE (1992). Recent chemical weathering of basalts. American Journal of Science 292 (10): 740-777.

Nozaki Y, Lerche D, Alibo DS, Tsutsumi M (2000). Dissolved indium and rare earth elements in three Japanese rivers and Tokyo bay: evidence for anthropogenic Gd and In. Geochimica et Cosmochimica Acta 64 (23): 3975-3982.

Patino LC, Velbel MA, Price JR, Wade JA (2003). Trace elements mobility during sphereroidal weathering of basalts and andesites in Hawaii and Guatemala. Chemical Geology 202 (3-4): 343-364.

Pokrovsky OS, Schott J, Dupré B (2006). Trace element fractionation and transport in boreal rivers and soil pore waters of permafrost-dominated basaltic terrain in Central Siberia. Geochimica et Cosmochimica Acta 70 (13): 3239-3260.

Prasad MS, Reid KJ, Murray HH (1991). Kaolin: processing, properties and applications. Applied Clay Science 6 (2): 87-119.

Qiu X, Liu Y, Alshameri A, Zhu X, Yan C (2017). Viscosity of kaolin slurries: effects of dispersant and urea-intercalation. Journal of Wuhan University of Technology-Material Science 32 (1): 51-57.

Rabiet M, Brissaud F, Seidel JL, Pistre S, Elbaz-Poulichet F (2005). Deciphering the presence of wastewater in a medium-sized Mediterranean catchment using a multitracer approach. Applied Geochemistry 20 (8): 1587-1596.

Rabiet M, Brissaud F, Seidel JL, Pistre S, Elbaz-Poulichet F (2009). Positive gadolinium anomalies in wastewater treatment plant effluents and aquatic environment in the Hérault watershed (South France). Chemosphere 75 (8): 1057-1064.

Rabiet M, Letouzet M, Hassanzadeh S, Simon S (2014). Transmetallation of Gd-DTPA by Fe^{3+}, Cu^{2+}, and Zn^{2+} in water: Batch experiments and coagulation–flocculation simulations. Chemosphere 95: 639-642.

Ryan W (1978). Properties of Ceramics Raw Material. 2nd ed. Oxford, UK: Pergamon Press.

Sabov Y, Said M, Tesfaye E, Haileyesus W (1985). Bombowoha kaolin and Kenticha Feldspar-Quartz deposits, Sidamo Administrative Region. Addis Ababa, Ethiopia: Geological Survey of Ethiopia.

Salvi S, Williams-Jones AE (1996). The role of hydrothermal processes in concentrating high-field strength elements in the Strange Lake peralkaline complex, northeastern Canada. Geochimica et Cosmochimica Acta 60 (11): 1917-1932.

Seto M, Akagi T (2008). Chemical condition for the appearance of a negative Ce anomaly in stream waters and groundwaters. Geochemical Journal 42 (4): 371-380.

Solodov NA, Semenov EI, Burkov VV (1987). Geological Handbook for Heavy Lithophile Rare Metals. Moscow, Russia: Nedra Press (in Russian).

Stocklin J (1977). Structural correlation of the Alpine range between Iran and Central Asia, Memoire Hors - Serie de la Societe Geologique de France 8: 333-353.

Strazzera B, Dondi M, Marsigli M (1997). Composition and ceramic properties of tertiary clays from southern Sardinia (Italy). Applied Clay Science 12 (3): 247-266.

Taylor SR, McLennan SM (1985). The Continental Crust: Its Composition and Evolution. 1st ed. Oxford, UK: Blackwell.

Uysal IT, Golding SD (2003). Rare earth element fractionation in authigenic illite-smectite from Late Permian clastic rocks, Bowen Basin, Australia: implications for physico-chemical environments of fluids during illitization. Chemical Geology 193 (3-4): 167-179.

Vegliò F, Passariello B, Toro L, Marabini AM (1996). Development of a bleaching process for kaolin of industrial interest by oxalic, ascorbic and sulphuric acids: preliminary study using statistical methods of experimental design. Industrial & Engineering Chemistry Research 35 (5): 1680-1687.

Verplanck PL, Taylor HE, Nordstrom DK, Barber LB (2005). Aqueous stability of gadolinium in surface waters receiving sewage treatment plant effluent, Boulder Creek, Colorado. Environmental Science & Technology 39 (18): 6923-6929.

Wang X, Jiao Y, Du Y, Ling W, Wu L et al. (2013). REE mobility and Ce anomaly in bauxite deposit of WZD area, Northern Guizhou. Journal of Geochemical Exploration 133: 103-117.

Zamanian H, Ahmadnejad F, Zarasvandi A (2016). Mineralogical and geochemical investigations of the Mombi bauxite deposit, Zagros Mountains, Iran. Chemie der Erde-Geochemistry 76 (1): 13-37.